Chapter 3

An investigation into an image model of topological texture

The previous chapter introduced an image model of topological texture (2.14). This model was used to predict relationships between surface relief, illuminant direction, and image texture — which, if valid, may have significant implications for texture classification. However, the model's derivation relied upon a number of assumptions associated with the projection geometry and the linearisation of the model. In addition shadowing of the surface was ignored. Thus the primary aim of this chapter is to investigate the validity of this model.

For natural textures the most restrictive of the assumptions made, in the author's opinion, are that slope angles are low and shadowing effects are not significant. Hence the investigation reported here paid particular attention to these two aspects.

Chapter 2 divided the model up into three components corresponding to the response of image texture to

(i)   changes in surface relief (i.e. changes in topological texture),

(ii)   changes in illuminant tilt angle, and

(iii)   changes in illuminant slant angle.

In addition to the above responses the model predicts that the radial shape of image magnitude spectra is a characteristic which is intrinsic to the underlying surface relief. That is, it is only a function of (i) and not a function of (ii) or (iii). Hence the objectives of this chapter are to assess the validity of the model by

(a)   investigating each of the responses (i) to (iii) above, and

(b)   investigating the intrinsic nature of the radial shape characteristic.

Thus this chapter is organised as follows. First, the response of image texture to changes in surface relief is examined. That is the relationship between the magnitude spectra of

surface relief and the magnitude spectra of image texture is investigated. Second, the response of image texture to variation in illuminant tilt and slant is presented, and the intrinsic nature of the radial shape characteristic is also examined here. Third and last, the conclusions of the chapter are presented and the implications for texture classification and segmentation re-examined.

3.1. The response of image texture to changes in surface relief

Chapter two's model of image texture (2.14) predicts that the radial shape of image magnitude spectra are determined solely by surface relief characteristics, and therefore may be an intrinsic characteristic of texture. Hence this section focuses upon this important relationship. It was investigated by synthesising height-maps of textures of varying spectra, simulating illumination, and examining the spectra of the resulting images. Physical experiments reported in later sections were used for the investigations into illuminant tilt and slant responses.

As fractal Brownian motion [Mandelbrot85] was used in the development of the image model [Kube88] it is also used here to model and synthesise surface relief. It has the advantages that it is easy to generate and provides natural looking images [Voss88] [Saupe88]. Compare for instance, figure 3.14 with figure 3.23.

The power spectrum of a two-dimensional fractal is of the form $f^{-\beta}$ where β is the power roll-off factor [Kube88], i.e. the log-log PSD plot is a straight line of a gradient of - β. Equation (2.12) implies that, for the fractal case, the power roll-off factor of the image texture (β_I) is related to the topological texture's power roll-off factor (β_H) by

$$\beta_I = \beta_H - 2 \tag{3.1}$$

and this is indeed the main conclusion of [Kube88]. Thus the investigation into the radial shape of texture spectra was restricted to the linear roll-off case. Initially the β relationship (3.1) was examined for a range of surface roll-off factors. The major concern however, was the effect of high slope angles and shadowing. Hence the second and third parts of the experiment investigated these aspects.

However, before the results are presented it is appropriate to describe the process through which they were created.

3.1.1. Image generation

An overview of the process used to generate all of the simulation results described in this chapter is given in figure 3.1.
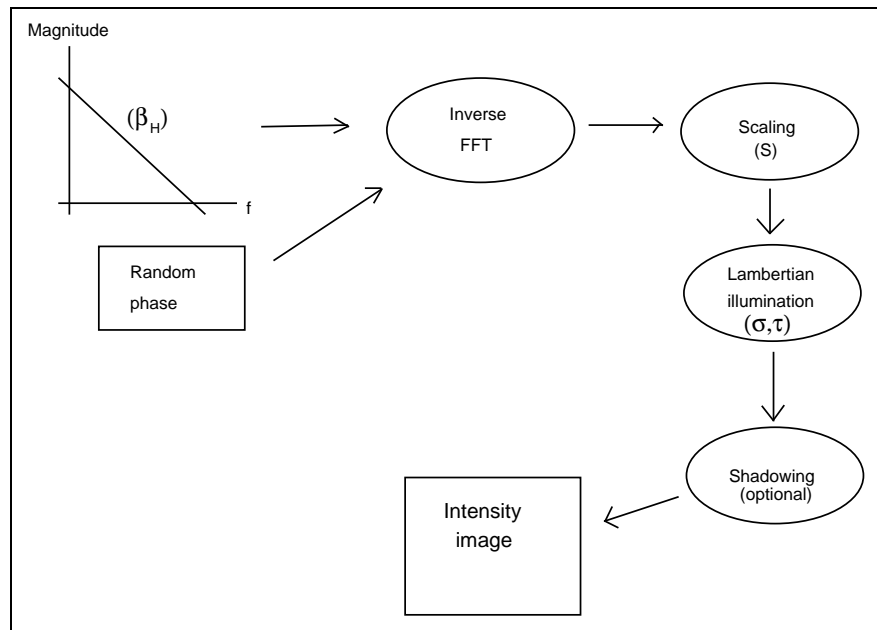

Figure 3.1 - Simulation process showing the major parameters (β_H, S, σ, τ)

All surfaces were synthesised using Fourier filtering [Linnett91a] [Saupe88]. A two-dimensional complex frequency spectrum was created with the desired isotropic power roll-off factor β_H and random phase. This was processed with an inverse Fast Fourier Transform (inverse FFT), and the resulting data where treated as a height-map for input into a Lambertian illumination program followed (optionally) by shadowing.

Details of the illumination program are as follows. The illumination vector was a constant over the scene. Orthogonal projection was used with the viewing direction parallel to the *z*-axis (as in the previous theory). A Lambertian shading model [Newman79] [Rogers85] was employed; the shading equation being derived from (2.1). Estimates of the surface normals ($\hat{\mathbf{n}}$) were calculated from local 2x2 neighbourhoods of height samples as defined below:

$$\hat{\mathbf{n}} = \left(\hat{n}_x, \hat{n}_y, \hat{n}_z \right) \tag{3.2}$$

where

$$\hat{n}_x = V_H(x, y) - V_H(x+1, y)$$
$$\hat{n}_y = V_H(x, y) - V_H(x, y+1)$$
$$\hat{n}_z = 1$$

Multiple reflections were not considered.

The parameters varied in the simulations presented in this chapter are :

β_H - roll-off factor of the log-log PSD of the surface (default 3.5),

S - height scaling factor – used to vary the surfaces' variance, and hence average estimated slope angle (default $S = 1$),

σ - slant angle of the illumination (default 50°), and

τ - tilt angle of the illumination (default 0°).

3.1.2. The power roll-off factor

The β relationship (3.2) relates power roll-off factors of topological and image textures. Implicit in this relationship is the assumption that the radial shape of the log-log PSD is a straight line, and that the gradient of this line (β) is an intrinsic characteristic of texture. This section reports an investigation into the β relationship (3.1) itself. The intrinsic nature of the PSD's radial shape is further investigated in following sections on slant and tilt angle responses.

A set of simulations was performed where only β_H was varied, the height scaling factor was kept at $S = 1$ (in order to reduce the effects of the non-linear terms), shadowing was not employed, and the lighting direction was kept constant at $\tau = 0°$ and $\sigma = 50°$. The power roll-off (β_I) of the resulting images was measured and the relationship between the two parameters estimated. Figure 3.2 shows three of the surfaces displayed as height-maps (where intensity represents height) and the corresponding intensity images. Mean radial sections of the two-dimensional magnitude spectra of the these height-maps and intensity images were obtained by averaging radial sections from $\theta = 0°$ to 180°. The resulting plots, together with least square estimates of power roll-off factors, are shown in figures 3.3 and 3.4.
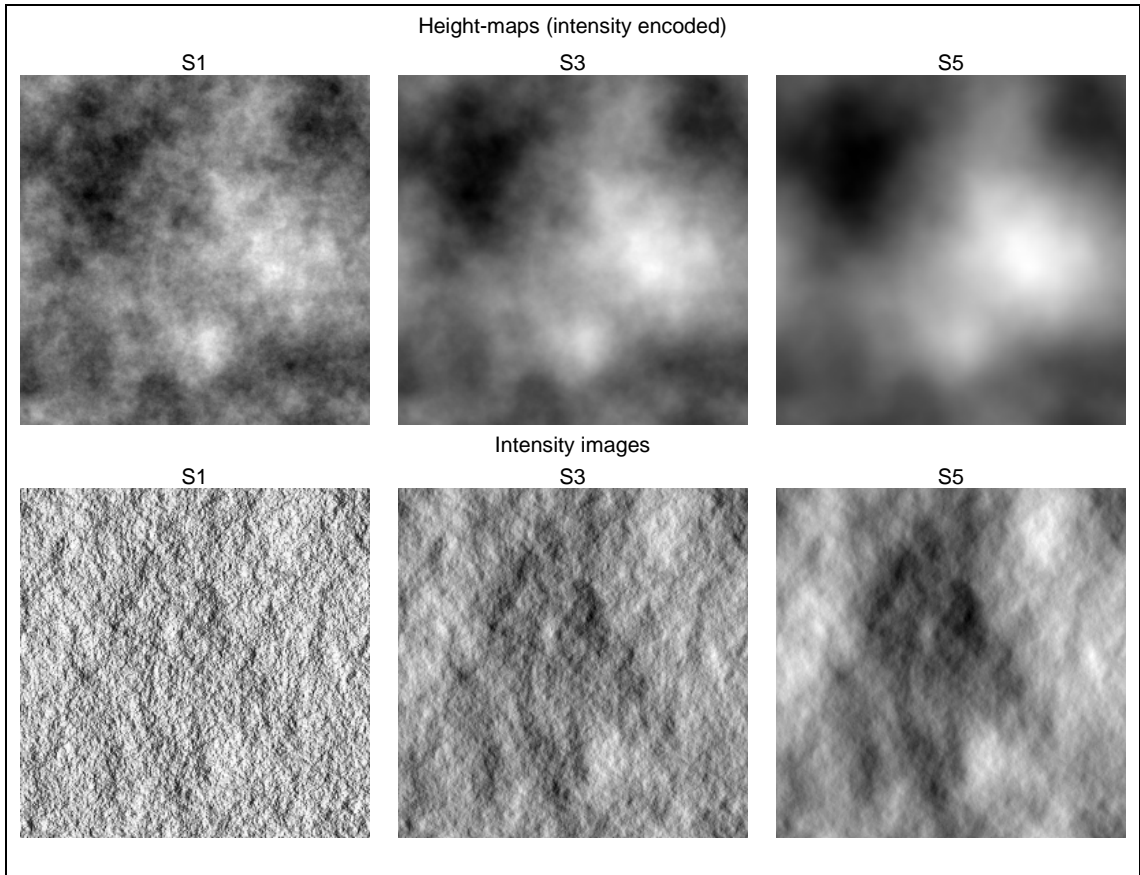
Figure 3.2 - Height-maps $V_H(x,y)$ of the surfaces, and their corresponding synthetically generated intensity images $I(x,y)$. The illumination source is to the right of the surfaces.
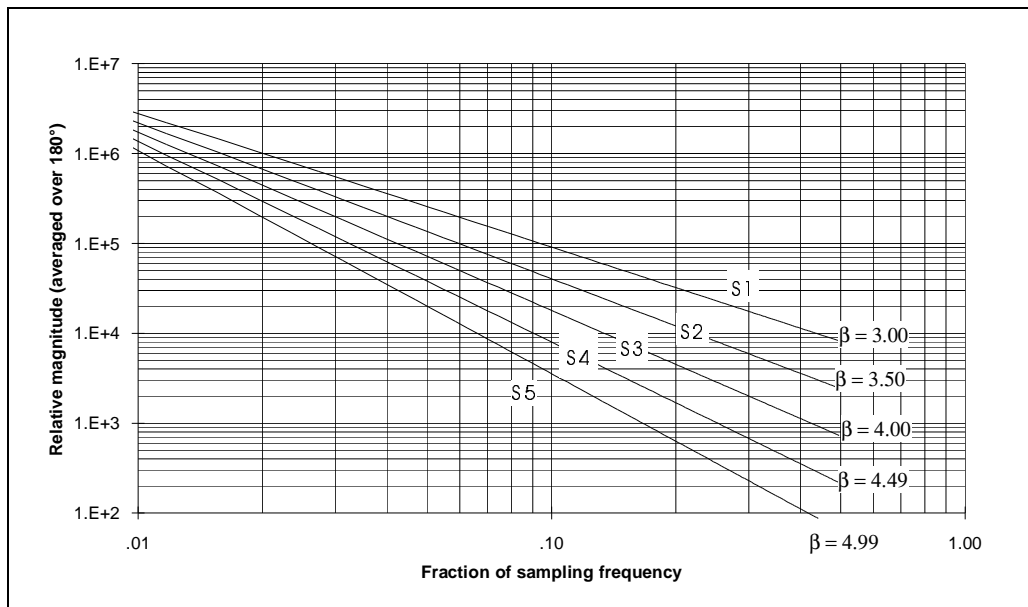

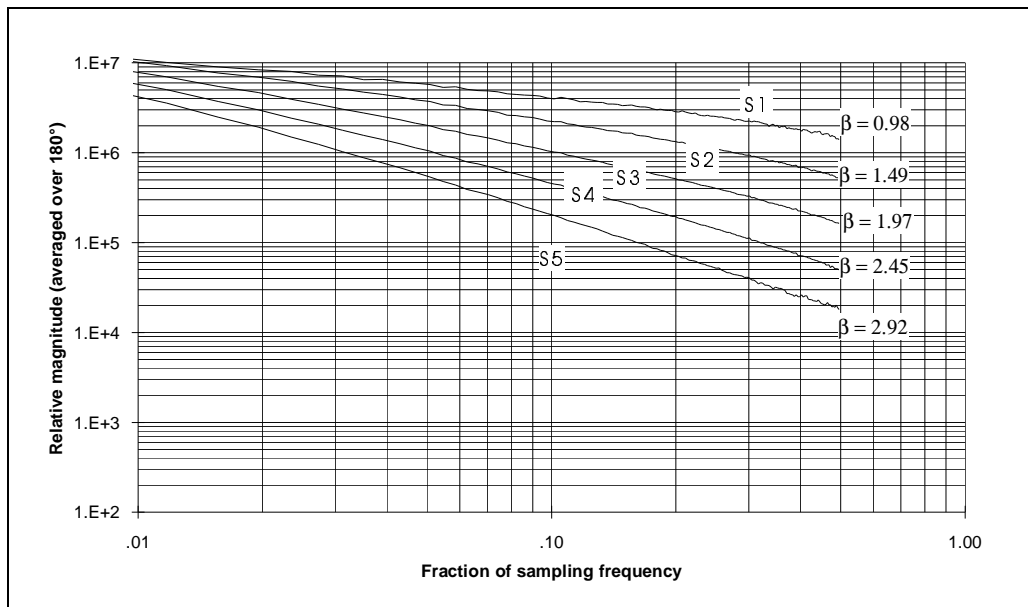*Figure 3.3 - Average radial sections of surface magnitude spectra shown with estimates of β_H.*

Figure 3.4- Average radial sections of intensity magnitude spectra shown with estimates of β_I.

The above show that both surface and image spectra have linear roll-off characteristics and that, as the theory predicts, the power roll-off factors of the images are approximately two less than their surfaces. Figure 3.5 shows this linear relationship more clearly. Here estimates of power roll-off factor of the images have been plotted against estimates of the original surfaces.
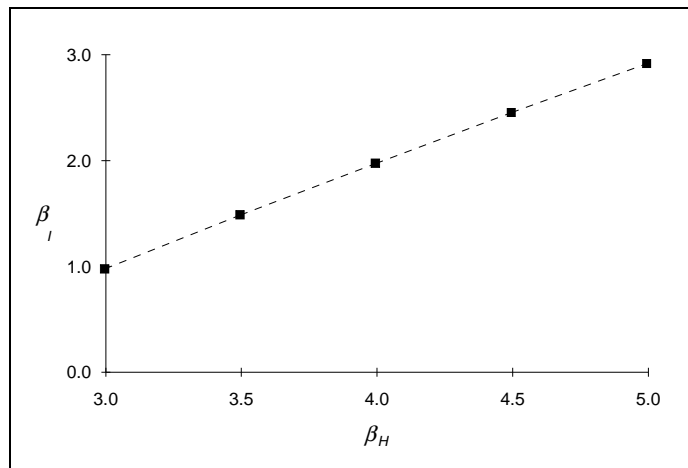
Figure 3.5 - β_I vs. β_H of surfaces S1 - S5.

The least squares estimate of a linear relationship between β_I and β_H (i.e. the best fit straight line to the graph shown in figure 3.5) is :

$$\beta_I = 0.97\beta_H - 1.92 \qquad\qquad (3.3)$$

- 32 -

This compares favourably with the β relationship (3.1) derived from the model. Note that the *average estimated slope angle* $(\hat{\alpha})$[1] varied between 2.5° for surface S5, up to 19.0° for surface S1. Thus the relationship between power roll-off factors of topological and image textures has been verified for low to moderate slope angles and no shadowing. The next two sections investigate each of these restrictions in turn.

3.1.3. Large slope angles

The use of the linear image model (2.14) presumes low slope angles and hence low height variance. In order to investigate the effect of larger slope angles the experiment reported above was repeated for increased surface variances. Height-map elements were multiplied by a height scaling factor (S) in the range 1 to 100, while β_H was kept constant at 3.5. The surfaces' *average estimated slope angles* $(\hat{\alpha})$, and *height variances* (s_H^2), are given in table 3.1. The *average estimated slope angles* $(\hat{\alpha})$ are calculated from the angles of the gradients between immediately neighbouring height samples in both x and y directions and averaged over the whole height-map (as defined below).

$$\hat{\alpha} = \frac{1}{n} \sum \frac{|\hat{\alpha}_x| + |\hat{\alpha}_y|}{2} \tag{3.4}$$

where

$$\hat{\alpha}_x = \tan^{-1}\left[V_H(x, y) - V_H(x+1, y)\right]$$
$$\hat{\alpha}_y = \tan^{-1}\left[V_H(x, y) - V_H(x, y+1)\right]$$

the summation is calculated over the depth-map, and

n is the number of samples contained in the depth-map.

The height variance is defined as :

$$s_H^2 = \frac{1}{n} \sum \left(\overline{V_H} - V_H(x, y)\right)^2 \tag{3.5}$$

where

$\overline{V_H}$ is the mean height of the surface.

---

[1]The average estimated slope angle $(\hat{\alpha})$ is defined in section 3.1.3

Height scaling factor (S)	1	2	4	10	20	40	100
Surface variance (s_H^2) in distance units^2	7	28	112	700.8	2,803	11,212	70,076
Average estimated slope angle $(\hat{\alpha})$	8.6°	16.2°	28.0°	47.5°	61.1°	71.5°	80.4°

Table 3.1. Average estimated slope angles and height variances, for surfaces with a range of height scaling factors (S)

Figure 3.6 shows sections through surfaces of different height scaling factors. Note that the surface with a height scaling factor of $S = 100$ has an average estimated slope angle of 80.4° and is therefore not typical of natural surface relief. Nevertheless it is still of value to investigate such extreme data, as they often exaggerate characteristics that might otherwise be overlooked.
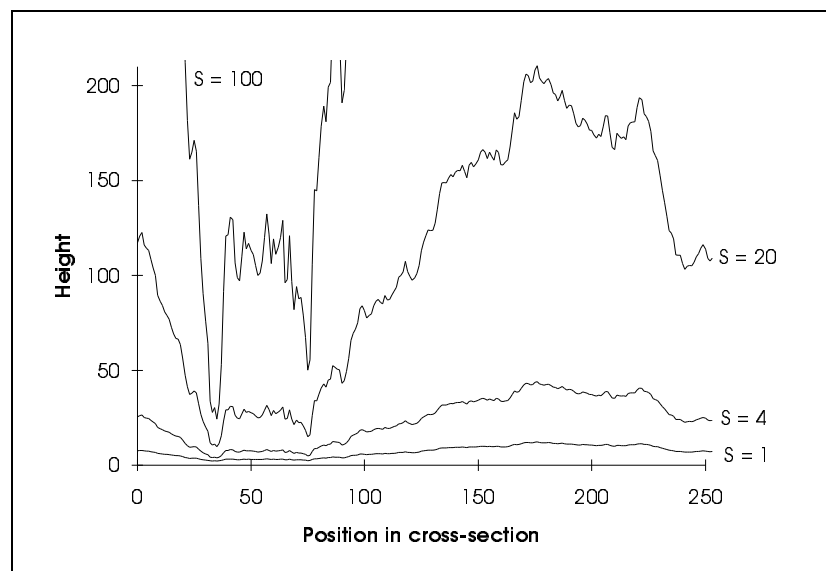
Figure 3.6 - Sections through four surfaces with height scaling factors S = 1, 4, 20 and 100 (note only part of S = 100 is shown for reasons of space)

Each of the surfaces listed in table 3.1 was used as input to the synthetic illumination process. Frequency spectra of the resulting intensity images are depicted in figure 3.7. They show that the gross shape is maintained, but that as the variance of the surface increases that of the corresponding intensity images saturates at a height scaling factor of $S = 20$. However, the image model (2.14) predicts that image variance is linearly related to surface variance. Not surprisingly, repeating the simulation with the linear illumination

scheme implied by the image model — i.e. using equation (2.4) — does not show this saturation effect. Hence it must be due to the quadratic and higher order terms of the Lambertian model (2.3) which are neglected in the linear image model (2.14).
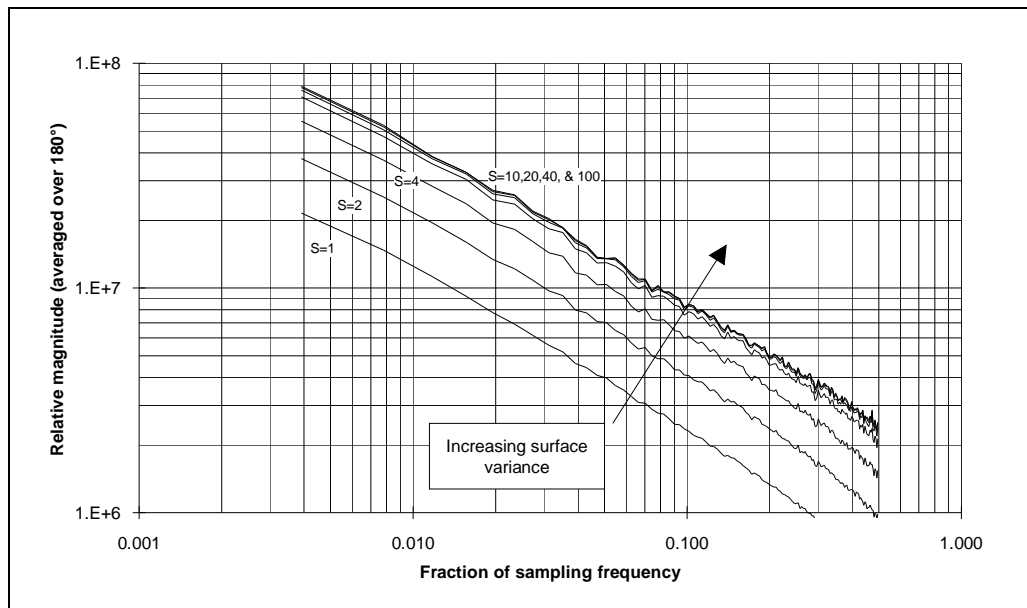

Figure 3.7 - Magnitude spectra of intensity images showing the effect of increasing surface variance.

This supposition is supported by figure 3.8. It shows the effect of increasing the amplitude of a sinusoidal corrugated surface on images generated using (a) the Lambertian model (2.3) and (b) the linear model (2.4). Clearly, as the magnitude of the surface is increased the energy of the intensity radiated by the Lambertian model is reduced compared with its linear companion.

Despite this saturation effect the gross radial shape remains constant over a wide range of average estimated slope angles.

As before roll-off parameters of the intensity images (β_I) were estimated and plotted against surface roll-off factor (β_H) to illustrate the β relationship at a variety of height scaling factors. For clarity the β relationships for only three height scaling factors are shown in figure 3.9. They show that although some deviation from the original relationship is introduced, it is surprisingly small.
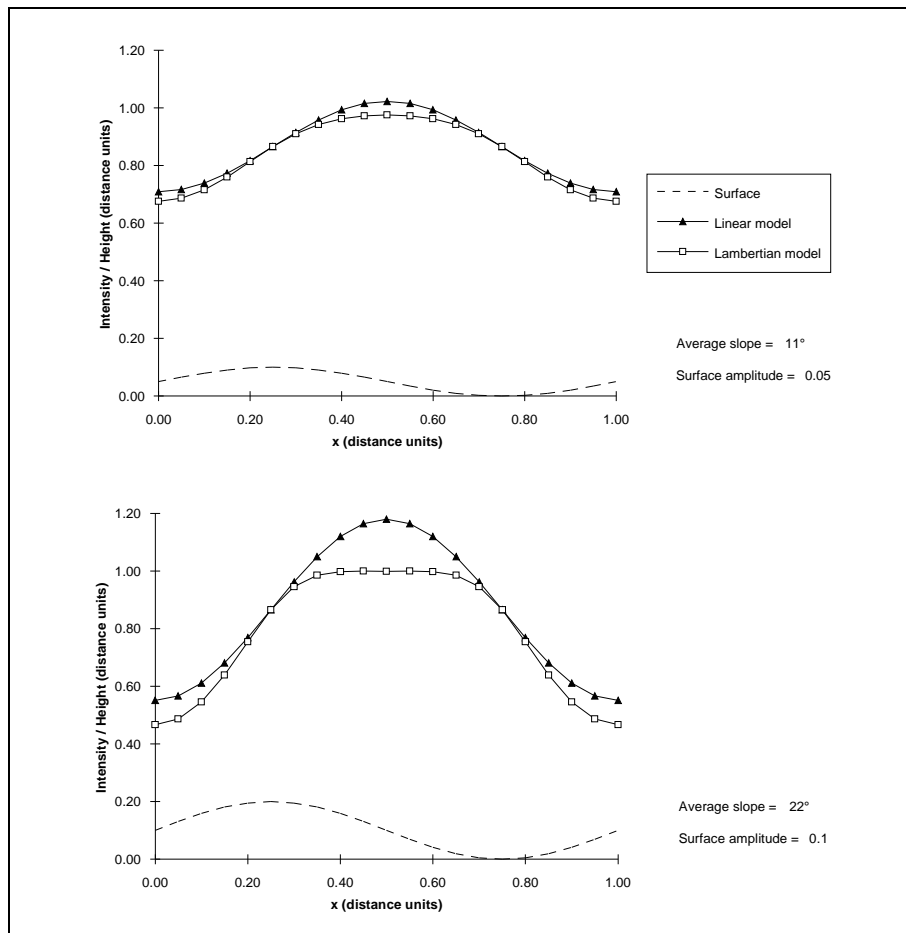
Figure 3.8 - The effect of increasing surface amplitude (from 0.05 to 0.10) on the intensity predicted by Lambertian and linear illumination models
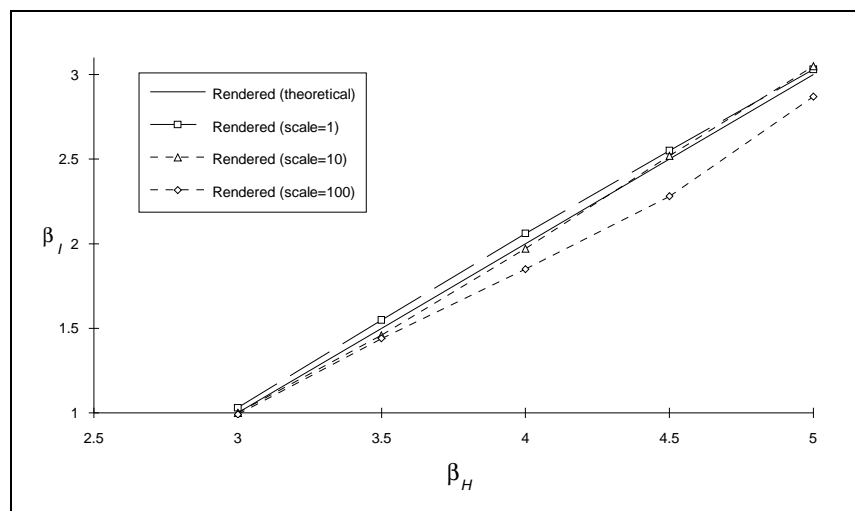

Figure 3.9- The β relationship at height scaling factors S = 1, 10, and 100.

3.1.4. Shadowing

After verifying the β relationship over a range of average estimated slope angles the experiments were repeated with the addition of shadowing. Shadowing was simulated by setting the intensity corresponding to a shadowed height-map sample to zero — thus no account was taken of multiple reflections. The two figures below show "shadowed" intensity images and their spectra for surfaces of constant power roll-off factor but varying height-map variances.
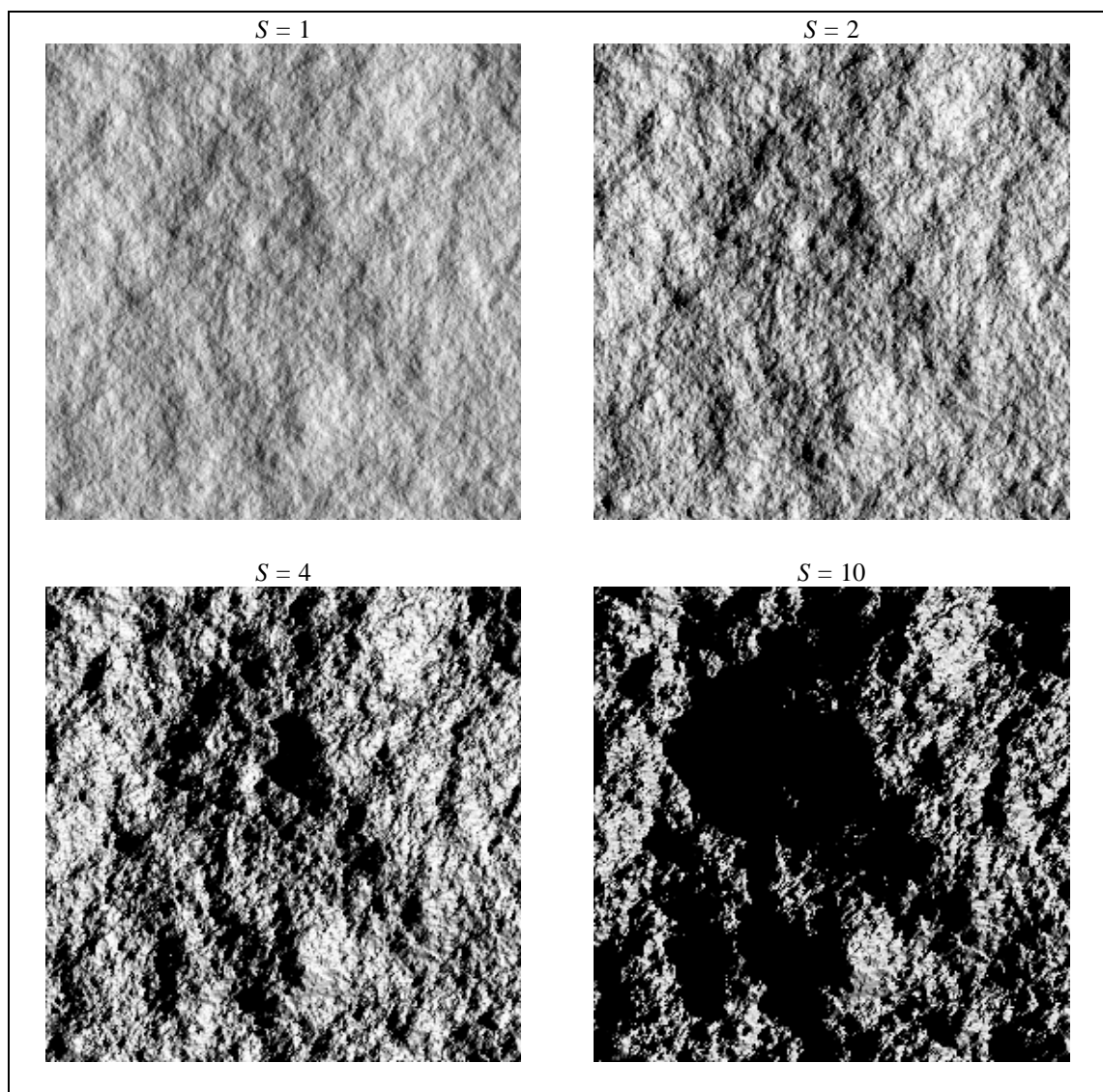
Figure 3.10 - Intensity images (with shadowing) of surfaces of varying height scaling factors (S=1, 2, 4, 10)
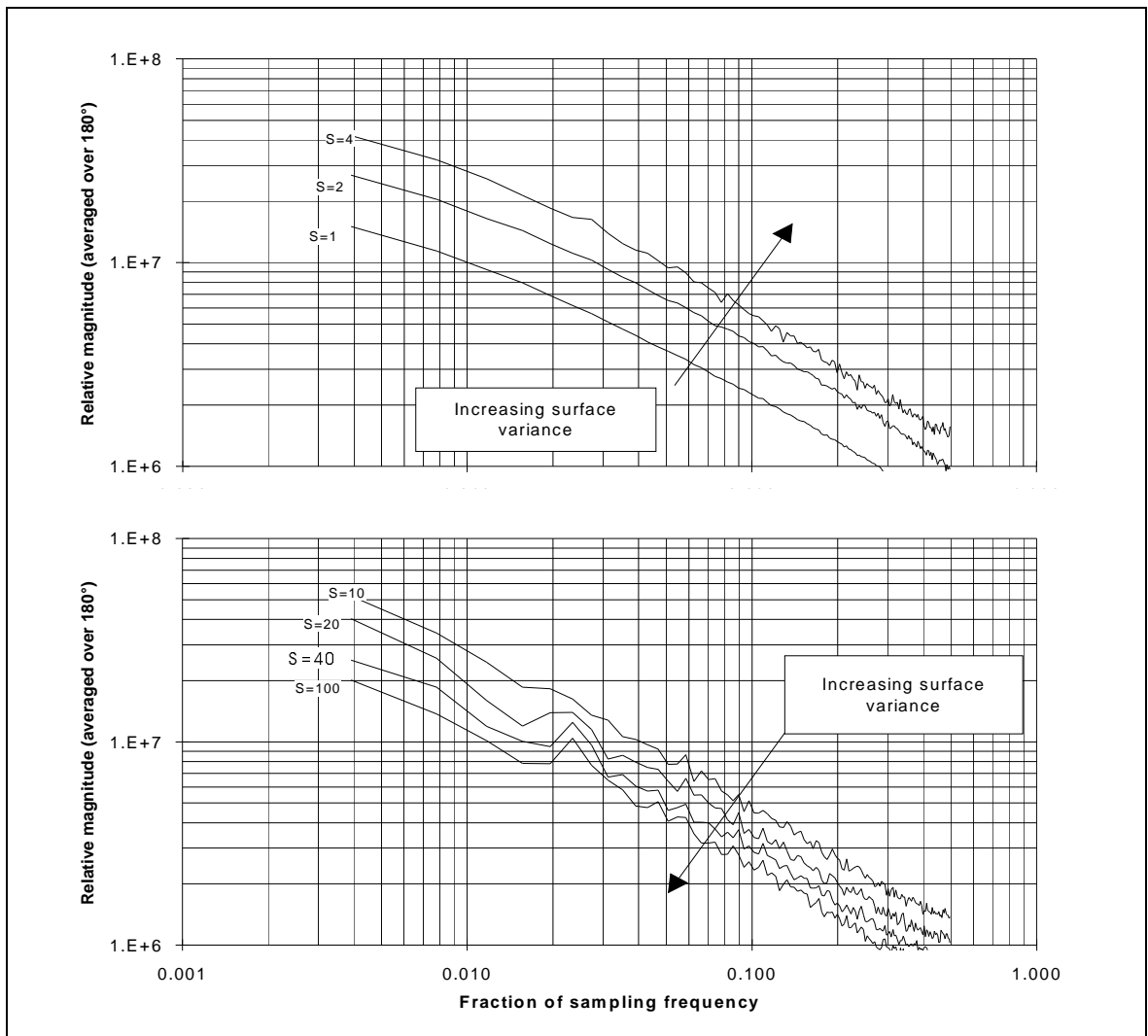
Figure 3.11 - Magnitude spectra of intensity images (with shadowing) showing the effects of increasing the variance of the surface (S = 1, 2, ...40, 100)

The magnitude spectra above illustrate that after a certain point (*S*=10 in the above case) the power spectral density of the intensity images actually decreases as the surface power is increased. However, as before, the straight line nature of the radial shape and its gradient remain largely unchanged.

For clarity figure 3.12 shows the β relationship for only three height scaling factors. From this graph it can be seen that the deviation from the predicted response is surprisingly small given that the theory did not take into account shadowing. This is especially so considering the high degree of shadowing that occurs for surfaces of higher variance — over 80% for a height scaling factor of 100.
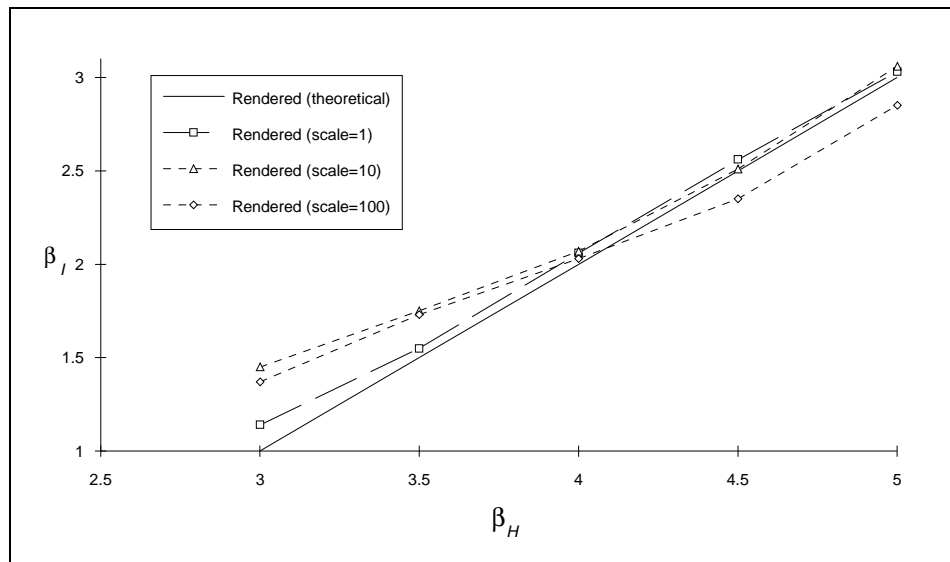
Figure 3.12 - Effect of shadowing, at different surface variances, on the β relationship.

3.1.5. Summary of surface response results

The previous sections have examined the relationship between characteristics of topological texture and image texture through simulation. Of particular interest was the radial shape of magnitude spectra, as the image model presented in chapter 2 predicts that this property is intrinsic to the surface, i.e. it is not affected by variation in illuminant vector. In the case where the radial shapes are straight lines with a roll-off factor β, the relationship reduces to (3.1) :

$$\beta_I = \beta_H - 2$$

It is this β relationship which was the subject of the investigations. Of particular concern was the effect of shadowing and high slope angles. The former had not been considered in chapter 2, while the latter was specifically precluded in order that a linear approximation could be used. The results presented have shown that high average estimated slope angles $\hat{\alpha}$ and shadowing make the simulation output deviate from that predicted by the linear model (2.14). The magnitude of the spectra saturated due to the inclusion of non-linear terms and even reduced when shadowing was included. However, the important result is that the gross radial shape of the spectra was not affected even for high $\hat{\alpha}$.

Thus these results show that for the simulation the β relationship is representative over a wide range of surface variance, but they do not however directly support the

suggestion that radial shape is an intrinsic characteristic of texture. The next two sections investigate the effect of variation of illuminant vector, and therefore allow such a proposal to be investigated.

3.2. The tilt angle response of image texture

The preceding section investigated the first part of the image model of topological texture (2.14), i.e. it investigated the surface response component (2.15). This section investigates the validity of the second part of the model — the tilt response component (equation 2.16) :

$$F_\tau(\omega, \theta) = \cos(\theta - \tau)$$

This predicts that the frequency components of a texture, in the same direction (θ) as the tilt angle of the illumination (τ), will be accentuated compared with those components at right angles to this illumination. Thus it implies that an image forming process using directed illumination acts as a *directional filter* of texture. Such an effect is likely to have important implications for texture classification schemes. It implies that the directional properties of image texture are not intrinsic to the surface, but that they are considerably affected by variation in illuminant tilt. This is unfortunate, as the majority of the feature sets reviewed in chapter 4 exploit directional characteristics.

Unlike the previous study, which was primarily required to vary surface relief in a controlled manner, the main requirement of this investigation is much simpler — that of varying the illuminant's tilt angle. Thus both simulation and laboratory experiment were used. Simulation was employed as before to selectively examine the effect of the non-linear terms and shadowing. Physical experiments were conducted to provide confidence that the simulations were reasonably representative of the behaviour of real texture, and to investigate a number of differing surface reliefs.

As with the discussion of the surface response, the tilt angle response is first investigated for low slope angles followed by an investigation into the effects of increasing the surface variance and the addition of shadowing.

3.2.1. Low slope angles

An isotropic surface was generated and illuminated synthetically as before ($S = 1$, $\beta = 3.5$, $\sigma = 50°$ & $\tau = 0°$). Figure 3.13 shows a polar plot of the FFT of the resulting image texture, in which each point on the graph represents the sum of the magnitude coefficients in one direction (i.e. for one value of θ : the angle of the frequency component).
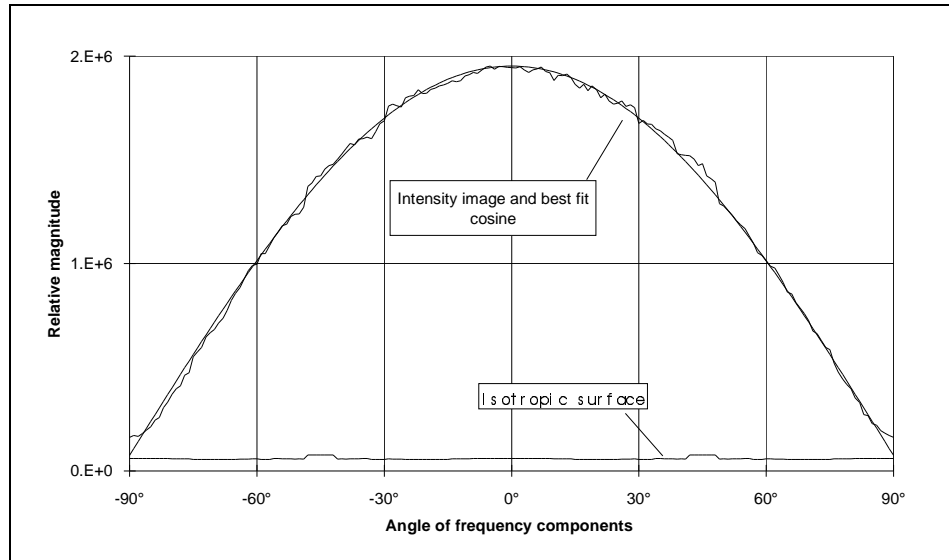

Figure 3.13- Polar frequency plot of image texture ($\tau= 0°$), and corresponding best fit cosine (original surface also shown).

The directionality in the image is clearly evident in the polar plot shown above, especially when the graph is compared to the almost flat plot of the original surface. As predicted by the image model the polar response is greatest in the direction of the illuminant tilt and it follows a cosine distribution very closely. However these data do not illustrate the effect of variation in illuminant tilt angle : figure 3.14 shows images for illuminant tilt angles of 0° and 90°.

τ=0°   τ=90°
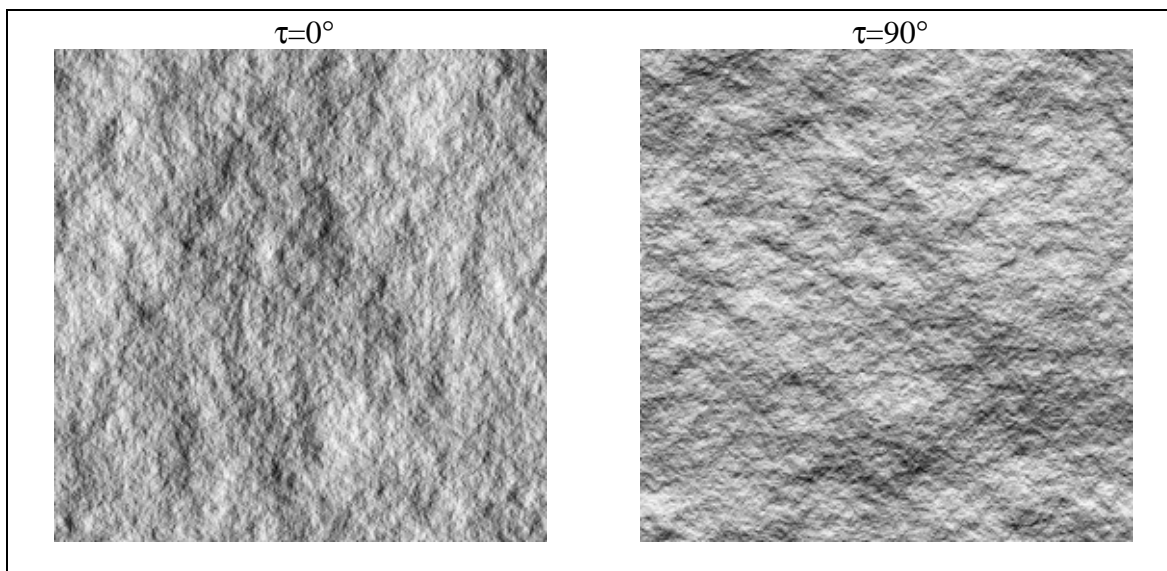
Figure 3.14 - Intensity images showing variation with tilt angle (τ)

The effect on these images could not be described as dramatic but it is clearly discernible. However, in the frequency domain the response to a change in tilt is much more obvious as shown in the polar plots below.
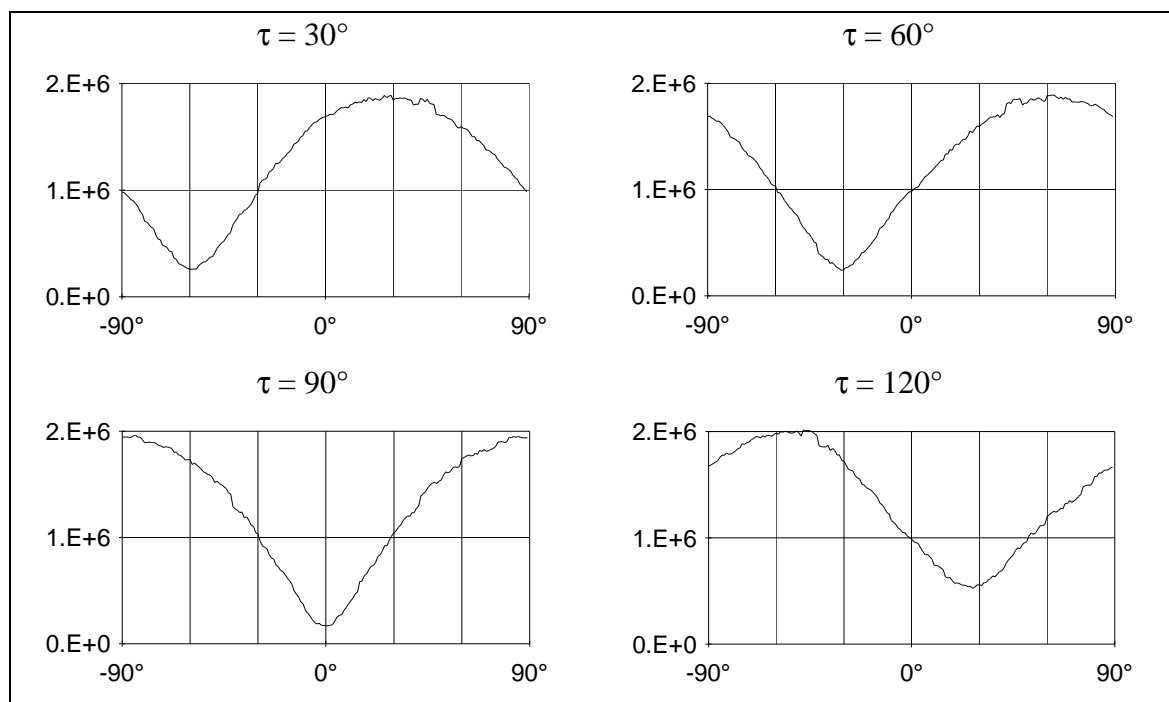
Figure 3.15 - Polar frequency plots of image texture showing the effect of variation in illuminant tilt (τ). Axes are as figure 3.13.

The above demonstrate that, in simulation, the tilt angle responses of images of isotropic topologies closely follow the directional characteristics predicted by the model. These

results are not surprising as the synthetic surface had an average estimated slope angle of 8.6° — and the effect of the quadratic and higher order terms neglected in the linear model(2.14) would be small. The next section therefore examines the effects of larger slope angles on the directional characteristics of image texture.

3.2.2. Large slope angles
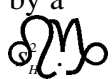
As before slope angles were increased simply by multiplying the original height-map by a height scaling factor (S), which naturally also increases the surface height variance σ_H^2. Figure 3.16 shows polar plots of the two dimensional magnitude spectra of the resulting images.
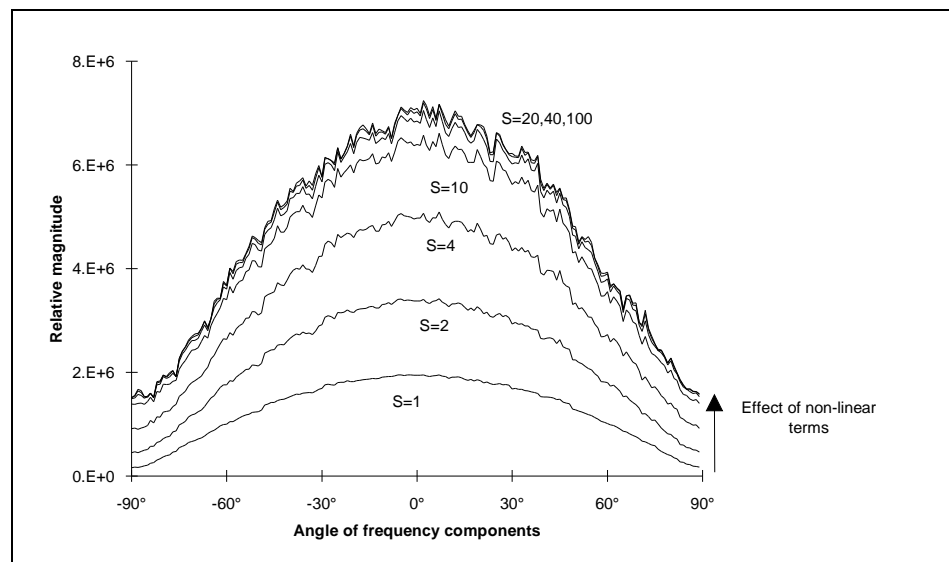
Figure 3.16- The effect of increasing average slope angles on the polar plots of magnitude spectra

These results show that large slope angles affect the cosine form of the image textures' directional characteristic very little. Increasing the surface variance increases image variance as predicted, except that, as was the case in the previous section on the β relationship, the image variance saturates at $S = 20$. This is due to the non-linear Lambertian illumination expression used in the simulation, as discussed in the previous section. However, the most interesting non-linear directional effects occur at $\theta = \tau \pm 90°$. Here the linear model predicts that *all* components will be filtered out, but figure 3.16 shows this is not the case. Repeating the simulation using the linear illumination model

removes the "saturation" and modified directional filtering effects, and shows that both are due to the quadratic and higher order terms of the Lambertian model (2.3).

If a surface consisting solely of components with a direction $\theta = \tau \pm 90°$ is considered, then

$$r = \frac{\partial V_H{}'}{\partial x'} = 0 \tag{3.6}$$

substituting (3.6) into the Lambertian model (2.3), and ignoring the mean term gives

$$I(x, y) = \cos \sigma \left[-\frac{t^2}{2!} + \frac{9t^4}{4!} \cdots \cdots \right] \tag{3.7}$$

Thus the image will also consist only of components at $\theta = \tau \pm 90°$. They are generated by the square and higher order t terms that are neglected in the linear model (2.14). For an image of an isotropic surface these terms will give rise to the "non-linear effects" seen at $\theta = \tau \pm 90°$ in figure 3.16, and will naturally become more significant at higher slope angles.

Therefore the "directional filtering" effect is reduced at higher surface variances. When shadowing is included it is further reduced as is shown in the next section.

3.2.3. Shadowing

As in the previous section, on the surface response, shadowing was investigated through the use of simulation. From figure 3.17 it is clear that shadowing only affects the polar plots significantly for height scaling factors of $S = 10$ and above. The polar plots of surfaces with a height scaling factor of $S = 4$ or less resemble their non-shadowed counterparts very closely. However, for surfaces with a height scaling factor of 10 and above, the variance of shadowed images actually reduces as the surface variance increases. This echoes the results obtained for the β relationship. Note however, that these polar plots still retain their cosine characteristic, but that they would be better represented by a raised cosine as the minima (at $\theta = \tau \pm 90°$) increase with surface variance. Thus the "directional filtering effect" is most severe at low slope angles.
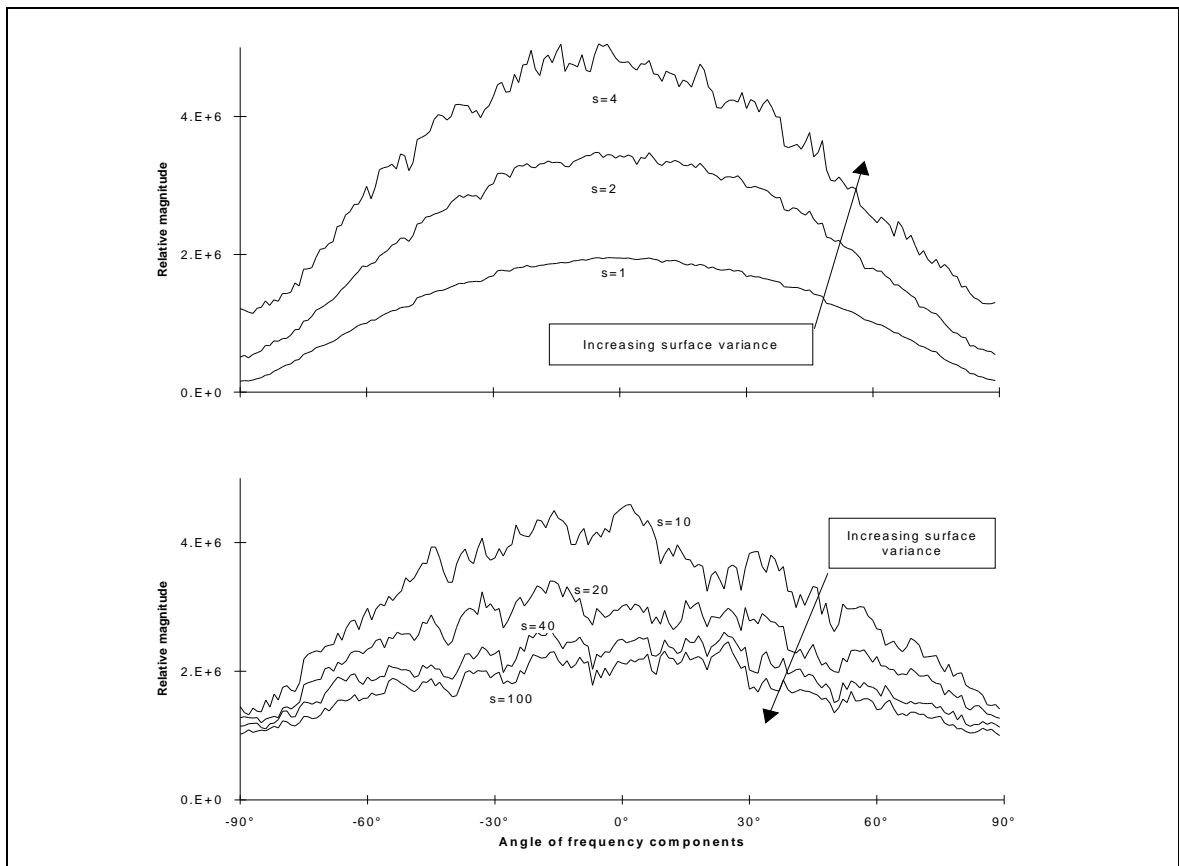
*Figure 3.17- Magnitude vs. angle of frequency components of **shadowed** images for various height scaling factors.*

3.2.4. Four physical textures

All of the results presented so far have been obtained via simulation. Its use has enabled the power roll-off and variance of surface textures to be precisely controlled in order that non-linear effects could be investigated. Shadowing has also been selectively investigated. These experiments would have been either difficult or impossible to perform with real textures. However, the exclusive use of simulation may result in false conclusions being drawn due to the incorrectness of either explicit or implicit assumptions. Hence in this section results of laboratory experiments are presented using four different samples of texture. These samples were selected using the following criteria :

(i)   The textures had to be isotropic in appearance to minimise their impact on the directional characteristics of the image textures.

(ii)   The "scale" of each texture had be such that it could (a) be detected by the imaging system, and (b) was not so large that a representative sample of it would not fit onto one of the 60 cm square mounting boards used in the experiment.

(iii)   The textures had to be of a material that could be spray painted.

(iv)   The texture samples had to be "globally" flat.

Images of the four textures are shown below in figure 3.18.

(a) "beans1" : a tray of butter beans   *(b) "chips1" : a tray of gravel chips*

(c)"stones1" a tray of beach pebbles   *(d) "rock1" : a small piece of conglomerate*
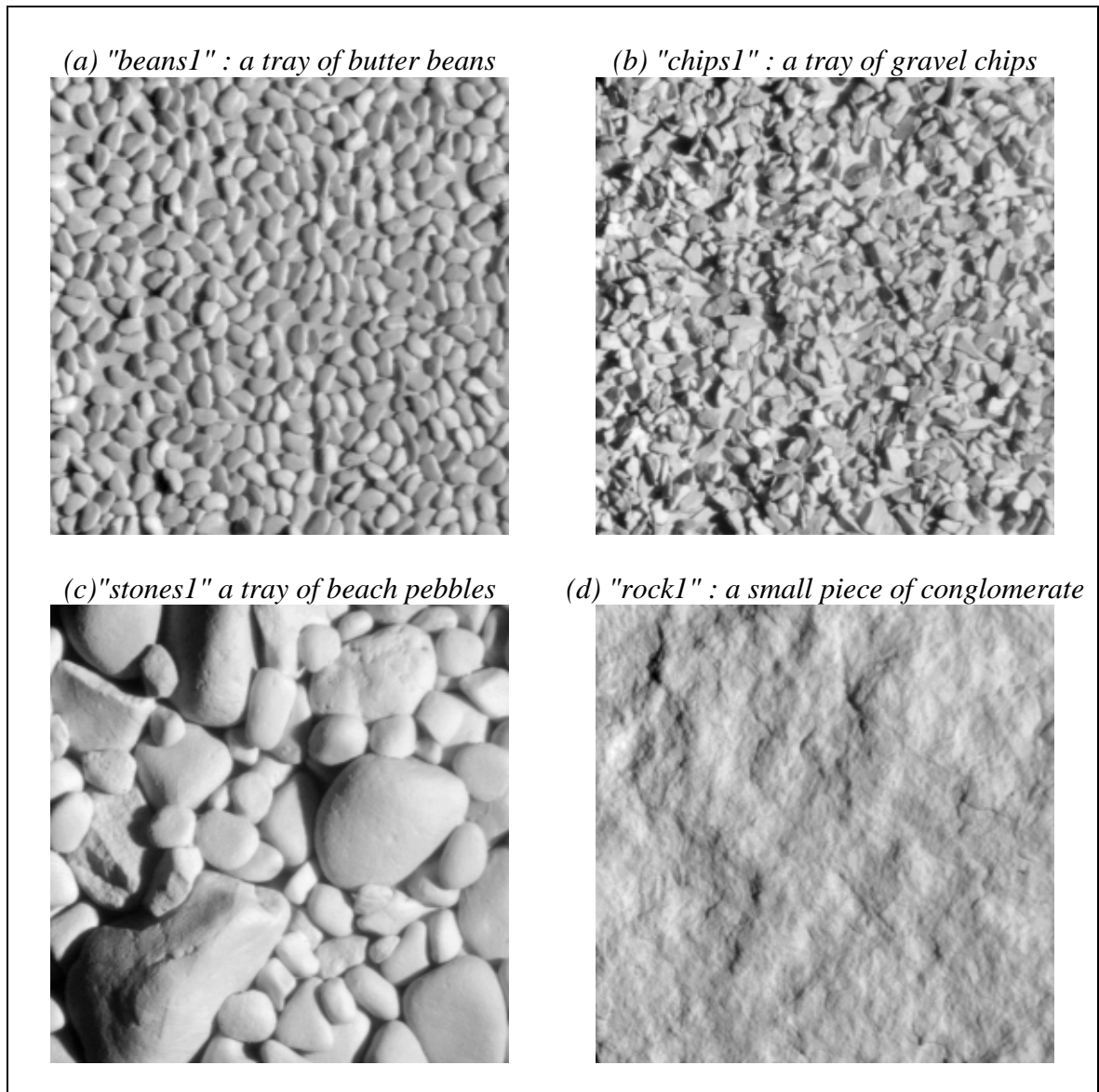
Figure 3.18 - The test textures.

If experimental results are to be of value then it is important that the phenomena that they exhibit are seen to be due to the process under investigation rather than the

experimental procedure or analysis. The following section therefore describes the experimental set-up and the analysis techniques employed after which the results are presented. As directional characteristics are important here special attention was paid to their possible artificial introduction, both in the capture of the images and the ensuing frequency domain analysis.

a)   Experimental technique

General set-up

Each of the textures was sprayed matte white to eliminate any albedo texture and to provide an approximately Lambertian reflectance characteristic. Images (512x512x8bit) were captured using a CCD[2] camera with a 40 mm lens (aperture = f11) connected to a frame store mounted in a workstation. The texture samples were mounted as shown in figure 3.19.
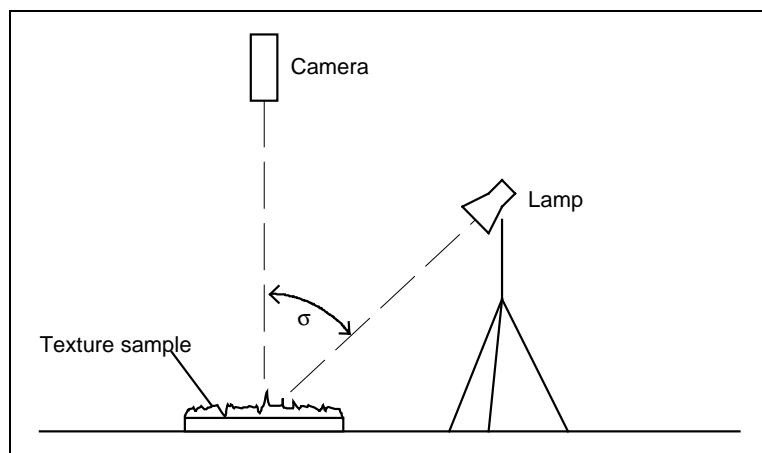
Figure 3.19 - Experimental set-up

That is they were mounted perpendicularly to the camera's line of sight at a distance of 3.3m; and illumination was provided by a 500W lamp, 1.6m from the subject. The position of the illumination was varied in terms of tilt and slant angles, and all other parameters were kept constant.

---

[2]Charge coupled device

Compensation for illuminant intensity variation

As the illumination source was mounted relatively close to the texture, and, as its lighting pattern was unknown, the variation in intensity of illumination incident on the textures' surfaces was investigated. It was especially important to remove any directional trends — as spectral leakage in the FFT process could *smear* the low frequency components due to the illumination trend to affect higher frequencies : thereby giving the illusion of a general trend over the whole frequency range. Variation in illumination was assessed by taking "registration images" of a flat matte white board;. A variation of 18% was observed in grey-levels. Registration images were therefore captured for each texture image and used to compensate for illumination intensity variation. Each texture image grey-value was divided by the corresponding registration grey-value.[3]

b)   Spectral estimation of image textures

The images shown in figure 3.18 are random in nature. Estimation of their spectra therefore becomes the problem of spectral estimation of random fields [Brigham88] [Marple87] [Kay81]. The main criteria for this estimation task are :

(i)   directional artefacts should be minimised,

(ii)   general trends of the spectra are more important than specific detail,

(iii)   *changes* from one magnitude spectrum to another, due to variation in illuminant tilt and slant angles, are more important than the absolute accuracy of the spectra themselves.

Unfortunately the raw application of a two-dimensional FFT routine to the image textures presents two problems : firstly the variance of the coefficients appears high relative to the underlying trend, and secondly large directional artefacts are introduced at $\theta = 0°$ and $90°$.

Directional artefacts

Directional FFT artefacts can be detected simply by rotating a digital image of texture and performing FFTs on the rotated and original images. Their polar plots (normalised with

---

[3]Note registration images were first normalised to a mean of 1.0 — by dividing each registration image pixel by the original registration image mean.

respect to θ) will then be identical except for any directional artefacts introduced. An example for the texture *rock1* for a 45° rotation is shown below.
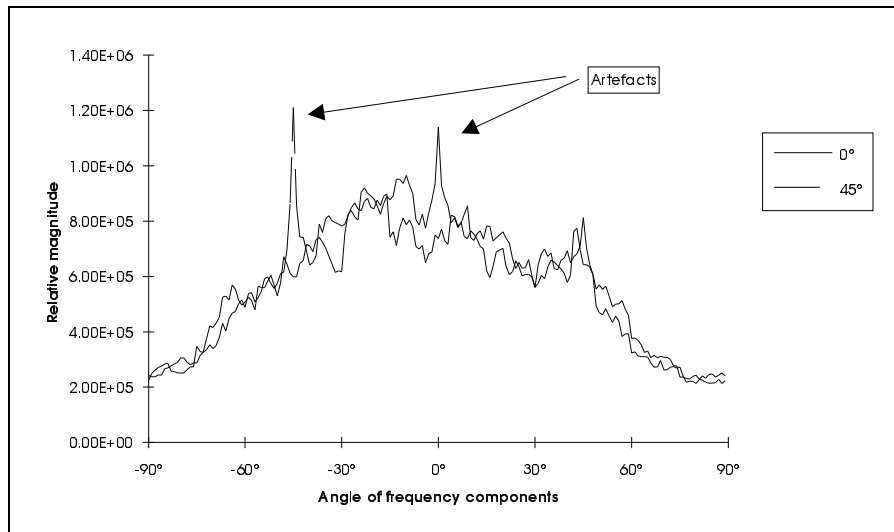
Figure 3.20 - Directional artefacts of raw FFT process

The above artefacts are caused by discontinuities formed by the straight edges of the image, and can be reduced by the application of a circular window [Huang72] [Brigham88, p252]. The next figure shows a sample of the results obtained by applying a circular window to a sequence of images.
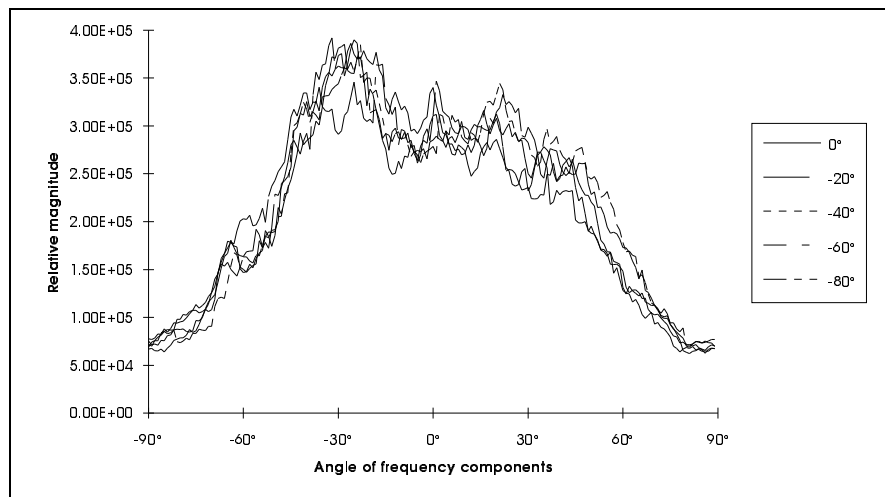

Figure 3.21 - Effect of a circular Hann window

These images were generated by rotating the camera about its viewing axis in 10° steps. Note that each plot has ben off-set by the appropriate camera off-set angle. All of the resulting polar plots were similar to the sample shown. Their similarity shows that no significant directional artefacts are introduced in either data capture or analysis *providing* a circular window is used.

Variance of Fourier coefficients

As the texture images are effectively random fields, it is not surprising that estimates of spectral coefficients obtained via the straight forward application of an FFT routine appear to exhibit high variance relative to the underlying trend. Standard methods of reducing variance of classical periodogram PSD estimators involve either spatial or frequency averaging. The Welch periodogram [Welch67] is straightforward to implement and has proven to be a robust estimator [Marple87]. It divides the data up into segments which overlap each other by 50%. The segments are windowed (using a circular Hann window) to reduce spectral leakage [Marple87], and transformed with an FFT to provide multiple periodograms which are averaged together. The figure below shows the radial sections of spectral estimates using three differing segment sizes. Note that a 512x512 image was used and so "one 512x512 segment" refers to a straight (non-averaged) FFT process. It has been plotted for comparison purposes.
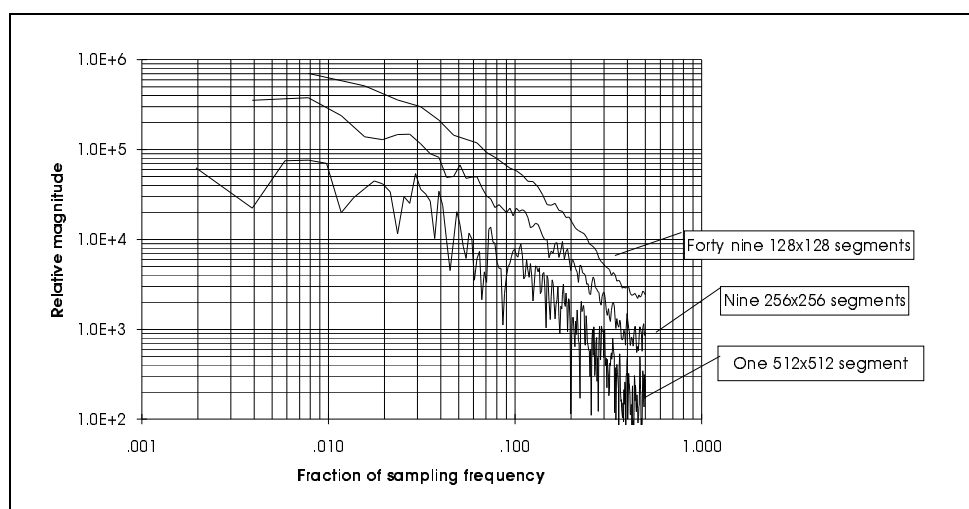
Figure 3.22 - Spatial averaging of magnitude spectra (note the spectra have been displaced vertically for display purposes)

The above figure shows that, as expected, reducing the segment size reduces the variance. In this thesis overall *trends* in response to illuminant variation are of interest rather than detail of spectra. The ability to reduce the "spread" of plots is valuable as it allows differences between graphs to be more easily observed, rather than being obscured by their own variance. Hence the Welch periodogram was used for the generation of all spectral estimates of images of physical textures.

c)   Tilt response : experimental results

The illuminant's tilt angle (τ) was varied in 10° steps over 180° for the four textures. The experimental set-up was as described in (a) above. Two examples of the resulting images are shown in figure 3.23. Magnitude spectra of the images were estimated using the Welch periodogram method using forty nine overlapping segments.   Examples of the polar plots of the two-dimensional spectra of *rock1,* are shown in figure 3.24.
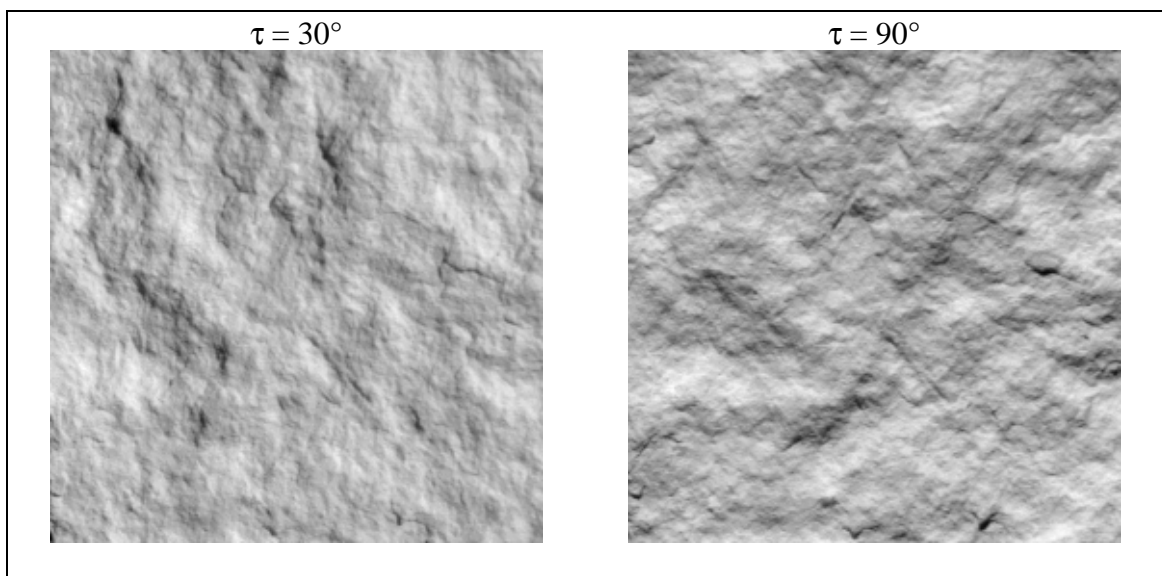
Figure 3.23 - Images of "rock1" captured at two different illuminant tilt angles

As predicted, illuminant tilt clearly has a considerable impact on directionality of image texture *rock1* (note that the angular position of the magnitude peak follows τ). What is perhaps more surprising however, is the similarity of the above plots to those obtained via simulation. Compare, for instance, the $\tau = 30°$ plot above with that of figure 3.15; both resemble a raised cosine and both have clear minima within a few degrees of -60°.
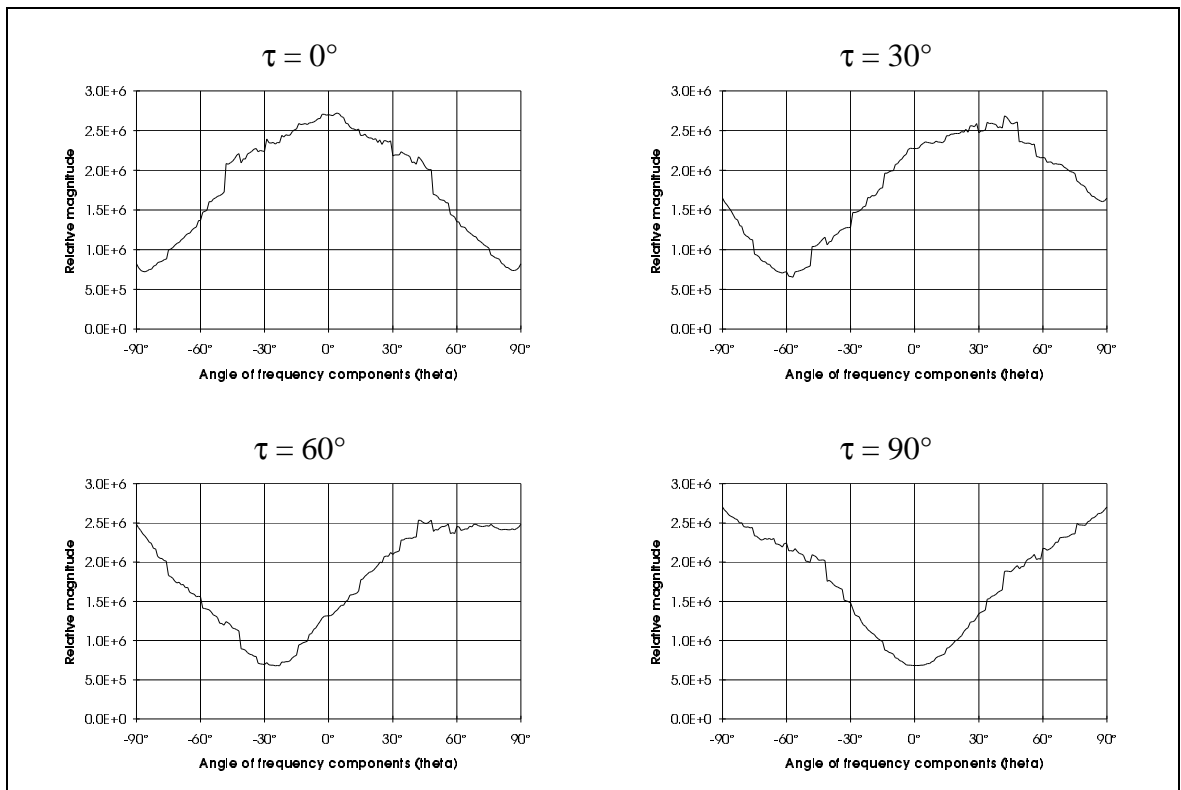
Figure 3.24 - Effect of illuminant tilt angle on image directionality (rock1)

The cosine relationship is more obvious in figure 3.25, in which magnitude has been plotted against $\cos(\theta - \tau)$.
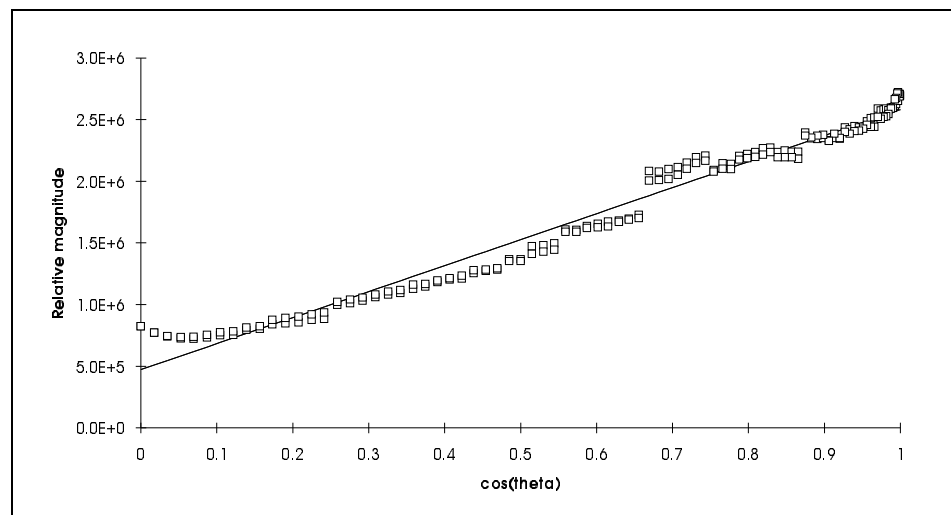
Figure 3.25 - cos(θ - τ) relationship for rock1, and best fit straight line
$$y = m_\tau \cos(\theta - \tau) + b_\tau \quad \text{(where y is the relative magnitude)}$$

It shows that there is an approximately linear relationship between magnitude and $\cos(\theta - \tau)$. Here the magnitude of the "platform" of the *raised* cosine can be determined

from the y-intercept of the graph (b_τ). The platform was caused in the simulation by non-linear terms — the height of the platform being related to the *average estimated slope angle* of the original surface. Increasing the slope angles increases the contributions of the non-linear terms and results in a higher platform. Thus if an image of a surface with apparently higher slope angles such as *stones1* were captured, its spectra would be expected to exhibit a higher platform. Table 3.2 below shows the slope and intercept estimates for all four textures including *stones1*. The estimates were obtained using least squares linear regression.

	rock1	beans1	chips1	stones1
slope(m_τ)	2.1E+6	2.2E+6	2.2E+6	1.7E+6
y-intercept(b_τ)	0.47E+6	1.7E+6	3.2E+6	2.7E+6

Table 3.2. Best fit raised cosine parameters for $y = m_\tau \cos(\theta - \tau) + b_\tau$

Figure 3.26 shows polar plots of the four image textures together with their best-fit raised cosines.
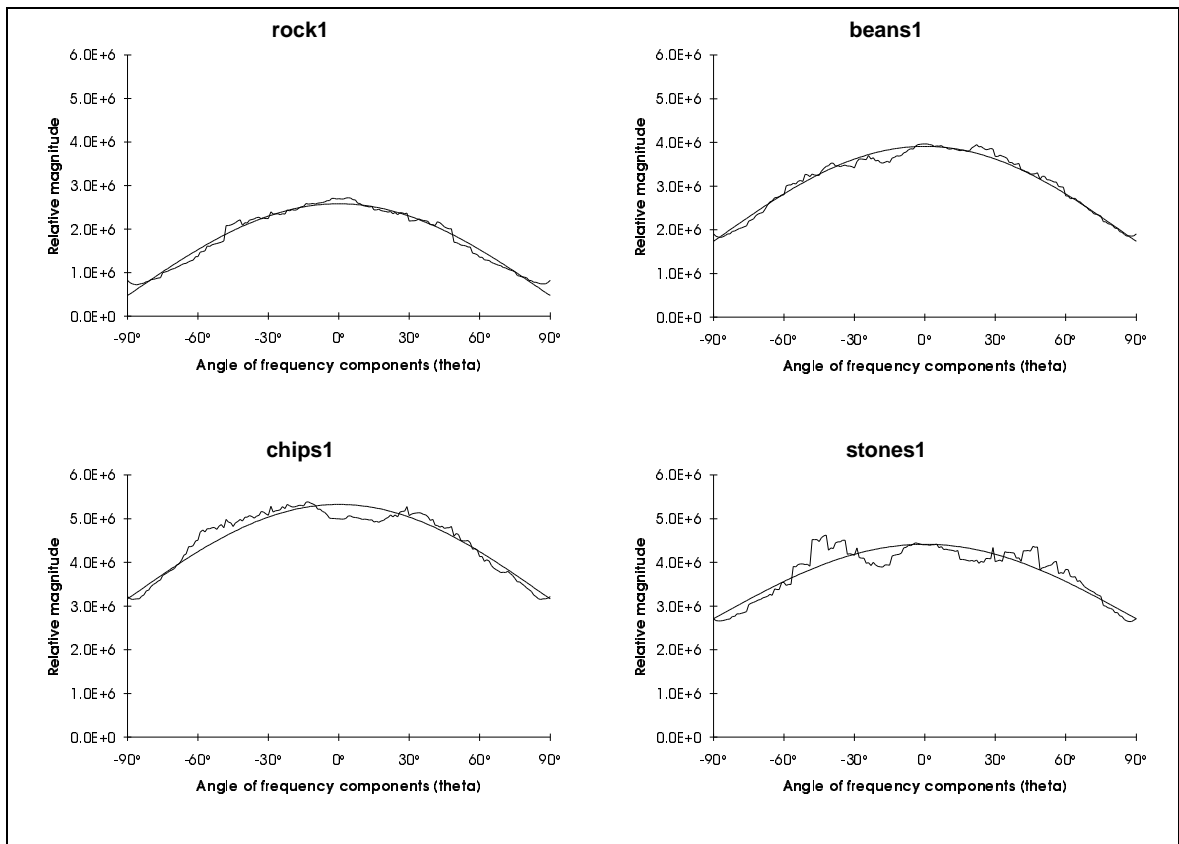
Figure 3.26 - Polar plots, and best fit cosines, of the textures beans1, chips1, and stones1 ($\tau = 0°$).

Table 3.2 and figure 3.26 show that *stones1* does indeed exhibit a higher platform than *rock1,* as do *chips1* and *beans1* — supporting the suggestion that the platform height is related to surface variance. This support however is tentative given the small sample and lack of quantitative surface height data. What is clear however, is that all four image textures exhibit distinct directional characteristics which "follow" the angle of tilt. These empirical results therefore

(i)   show that image texture directionality is not an intrinsic characteristic, and

(ii)   support the $\cos(\theta - \tau)$ relationship between illuminant tilt and image texture, but show that it should be more accurately modelled by adding an additive term to account for the raised cosine effect. That is it shows that the tilt component should be modified to :

$$F_\tau(\omega, \theta) = m_\tau \cos(\theta - \tau) + b_\tau \tag{3.8}$$

d)   Radial shape - an intrinsic characteristic ?

The above shows that the directional characteristics of image texture are not independent of illuminant tilt — as predicted by the image model presented in chapter 2. This model also predicts that radial shape of magnitude spectra is an *intrinsic* property (see figure 2.5). If this is indeed the case it will be independent of illuminant tilt. Thus radial plots of image texture will show that variation in tilt changes the level but not the form of the log-log radial response. Figure 3.27(a) shows the response of *rock1* image texture to variation in illuminant tilt (τ). It contains radial sections through the periodograms at an angle $\theta = 0°$. These sections show that, as predicted by the image model (2.14), the magnitudes reduce as τ deviates from θ, and that the plots are similar to each other in shape although they converge towards each other at the Nyquist frequency.

Figures 3.27 (b), (c) and (d) show radial sections of the other three isotropic textures. These plots together with those at other values of θ all show similar results — gross radial shape is maintained but the plots converge as the Nyquist frequency is approached. That is the gradients of sections (particularly of *beans1* and *chips1*) are dependent upon the tilt angle of the illuminant. Hence, contrary to predictions derived

from the image model (2.14), estimates of the power roll-of factors of these textures would not in this instance provide a feature which is independent of illuminant tilt angle.

a) rock1   b) beans1

c) chips1   d) stones1

τ = 0° (top traces), τ = 30° (2nd top traces), τ = 60°(2nd bottom traces), τ = 90° (bottom traces)
θ = 0°, σ = 50°.
Axes as for figure 3.24
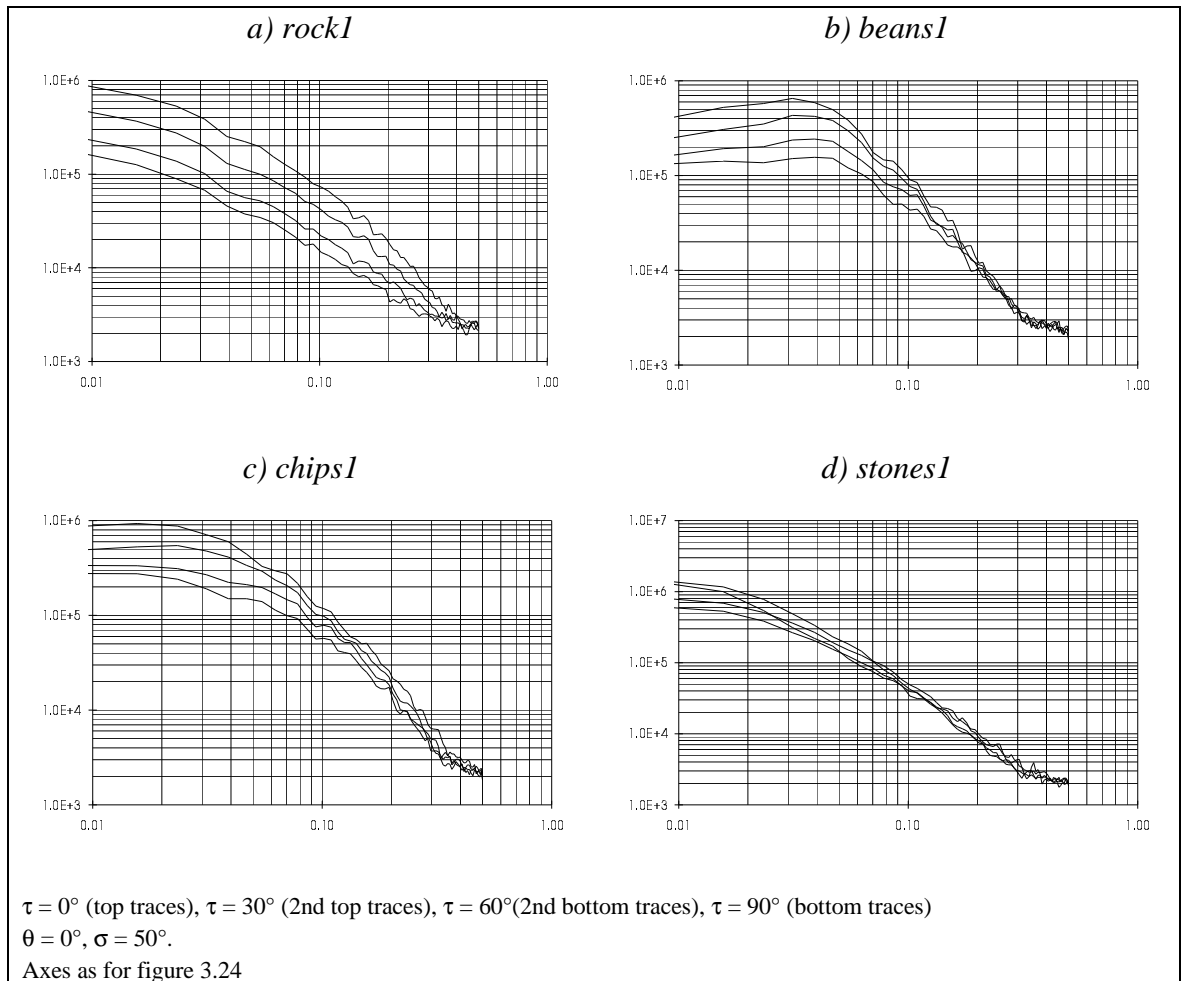
Figure 3.27 - Effect of tilt on radial shape of magnitude spectra (axes as previous figure)

3.2.5. Summary of tilt response investigation

This section has presented the results of an investigation into the effects of variation in illuminant tilt angle, on image texture; through the use of simulation and laboratory experiment. To summarise :

- Results from simulation and experiment show that the directional characteristics of image texture are not intrinsic — but that they are dependent upon illuminant tilt.

- The linear image model (2.14) predicts a pure cosine relationship : $\cos(\theta - \tau)$ but the results of simulation and laboratory experiment show that a raised cosine : $F_\tau = m_\tau \cos(\theta - \tau) + b_\tau$ — is more appropriate for textures with larger slope angles.

- The shapes of radial sections of the test textures at different illuminant tilt angles are similar, although convergence of the sections towards the Nyquist frequency was observed. Thus in this instance estimates of the power roll-off factor β are not independent of the tilt angle of the illuminant.

3.3. The slant angle response of image texture

The two preceding sections of this chapter have investigated the response of image texture to variations in surface relief and illuminant tilt angle (τ). The results presented support the first two parts (F_s and F_τ) of the image model of topological texture (2.14). The third component of the model concerns the response of image texture to changes in illuminant slant angle (2.17) :

$$F_\sigma = \sin \sigma$$

This implies that, as the angle the illuminant vector makes with the vertical is increased, the whole magnitude spectrum is uniformly amplified by a factor equal to the sine of that angle.

The aims of this section are therefore :

(i)   to assess the validity of the slant response predicted by (2.17), and

(ii)   to further investigate the intrinsic nature of the radial shape of image texture magnitude spectra.

As in the previous section, simulation was used to gain an insight into the effect of high slope angles and shadowing, while laboratory experiment provided results with real textures. The intrinsic nature of PSD radial shape is discussed again here — from the perspective of slant angle response; and the section finishes with a summary.

3.3.1. Low slope angles

Synthetic images of texture were generated as described in section 3.2.1 using low average slope angles (height scaling factor $S = 1$). For these simulations the illuminant's tilt (τ) was kept constant at 0°, while the slant angle (σ) was varied in 10° steps between

10° and 80°. Figures 3.28 and 3.29 show samples of four of the resulting images and their magnitude spectra.
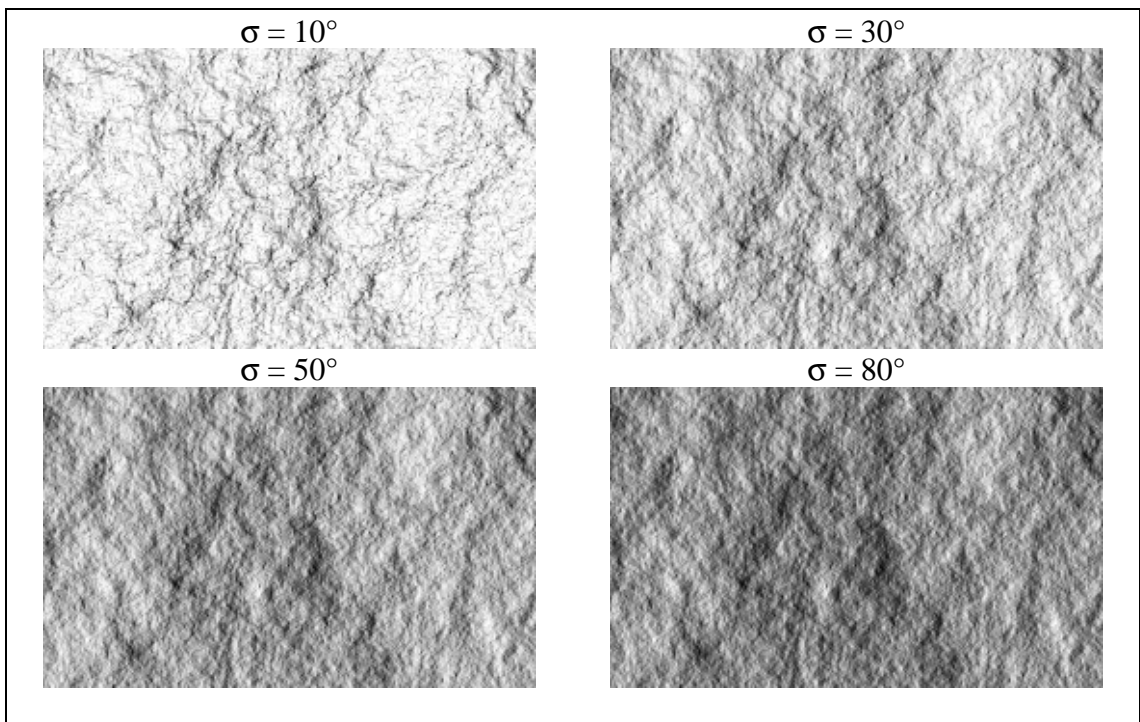
Figure 3.28 - Samples of intensity images — showing the effect of changing σ.
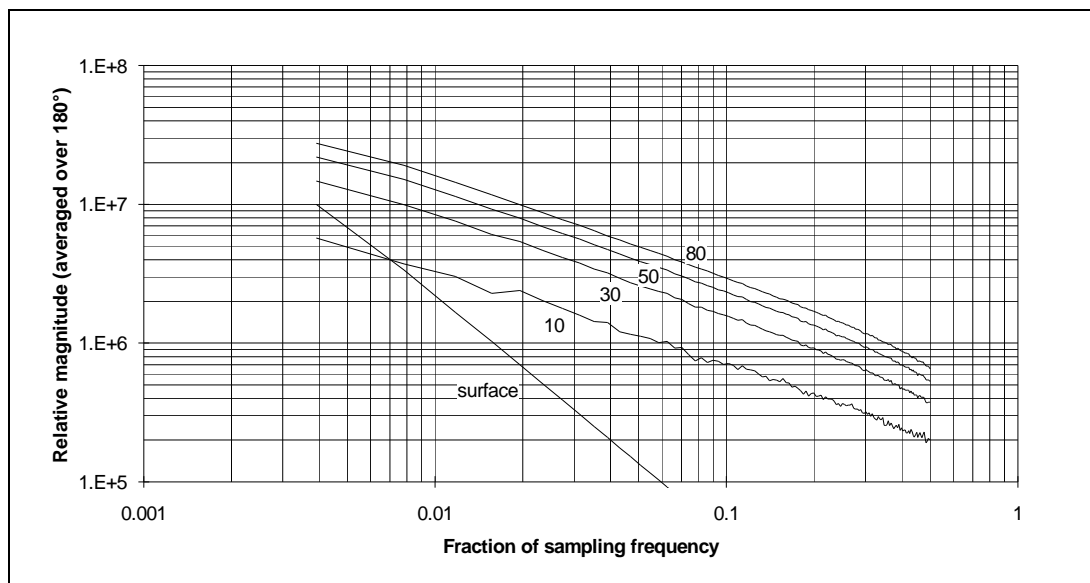
Figure 3.29- Frequency spectra of surface height map and intensity images for σ= 10ᶜ, 30ᶜ, 50ᶜ, and 80ᶜ.

As predicted by the image model (2.14) the slope of the above spectra do not change (i.e. the power roll-off factor β_I remains constant) but the variance of the image texture does increase with slant angle (σ). In order to establish whether equation (2.17) represents the slant angle response, magnitudes of frequency components (at $\omega = 0.12\omega_S$) were estimated for each image[4]. These estimates were calculated using the least squares fit of a straight line to the log-log magnitude spectra. They are plotted against sin σ in the graph below.
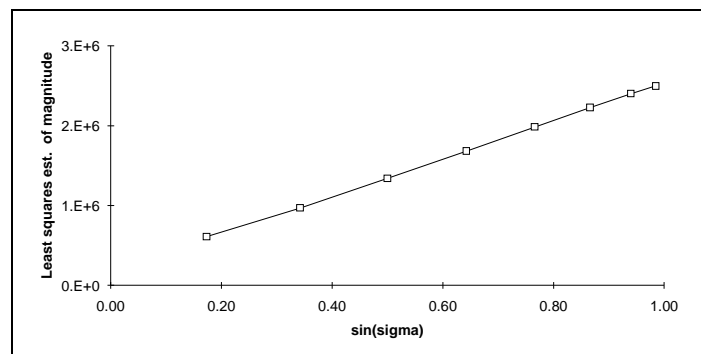
Figure 3.30 - Slant angle (σ) response showing the sinσ relationship   (for $\sigma=10^{c},20^{c}...80^{c}$).

The above graph shows that the simulated magnitude response is a linear function of   sin σ as predicted by the image model (2.14).

3.3.2. Large slope angles and shadowing

The simulations were repeated for a variety of surface variances in order to test the applicability of the slant angle relationship for larger slope angles. Figure 3.31 shows that the relationship remains linear, although it is obvious that the y-intercept constant increases with surface variance.

Unfortunately this linear relationship does not continue to hold once shadowing has been introduced. Figure 3.32 shows images at the same slant angles as before, but for a surface variance of 112 ($S = 4$) and with the addition of shadowing.

---

[4]Where ω_S is the sampling frequency.
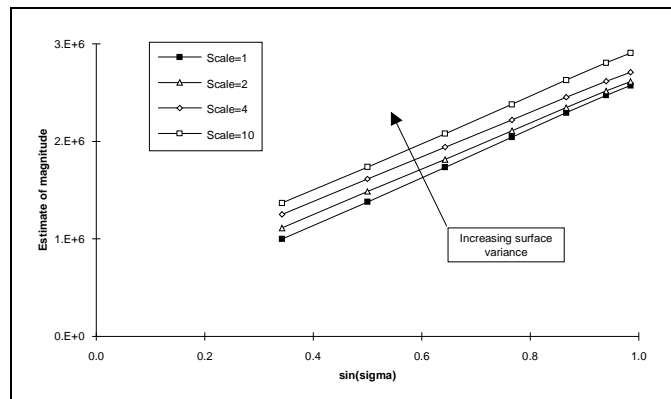
Figure 3.31 - Effect of power (scale = 1, 2, 4 & 10) on slant angle response
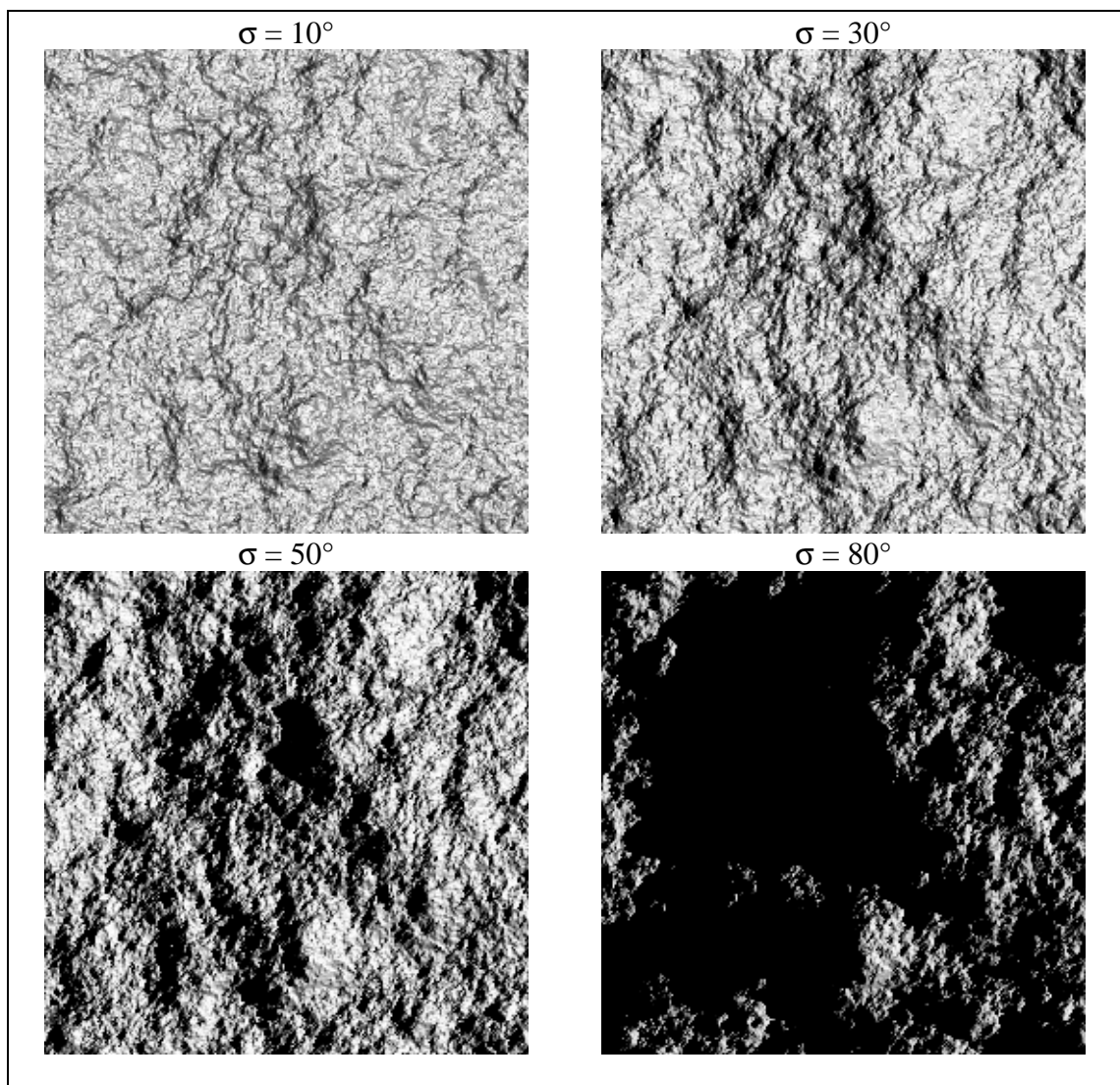
Figure 3.32 - Intensity images showing variation due to change of slant angle for a height scaling factor S = 4

As the graph below shows adding shadowing to the simulation severely distorts the linear relationship.
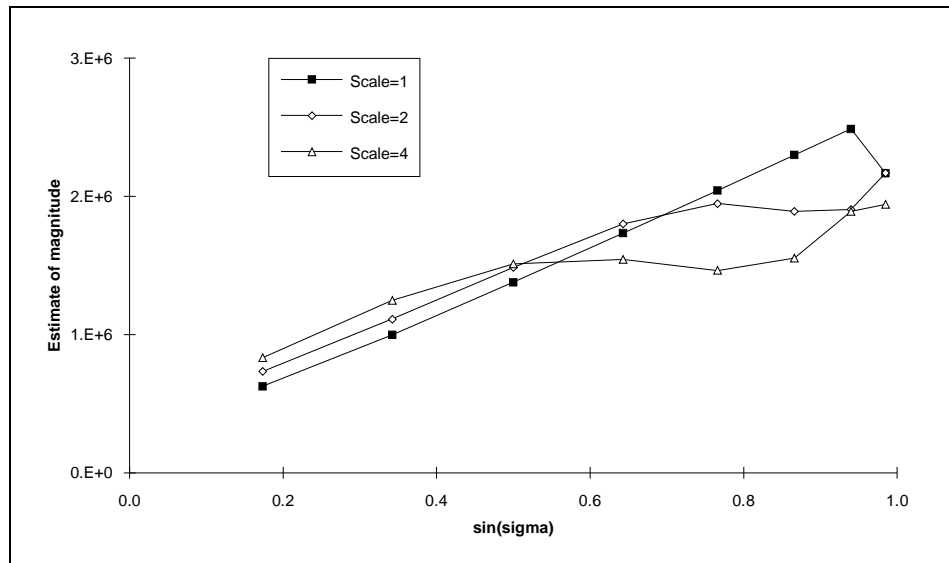
Figure 3.33- Effect of shadowing at various powers (scale = 1, 2 & 4) on the slant angle response.

For each of the height scaling factors shown, a significant reduction in magnitude occurs when the area in shadow exceeds 1-2%. Thus the slant angle response is severely modified by even slight shadowing.

In conclusion therefore, simulation results predict that "sin σ" slant response holds while the degree of shadowing is small, but that it is severely affected by even small amounts of shadowing.

The following section therefore investigates this relationship using four real textures.

3.3.3. Experimental results : slant response

The four textures used in the tilt angle experiments; *rock1, beans1, chips1,* and *stones1,* were imaged as before, except that illuminant tilt was kept constant at $\tau = 0°$, and slant was varied in 10° steps between 10° and 80°. Four samples of the resulting intensity images and their magnitude spectra are shown in figures 3.34 and 3.35.

σ=10°   σ=30°

σ=50°   σ=80°
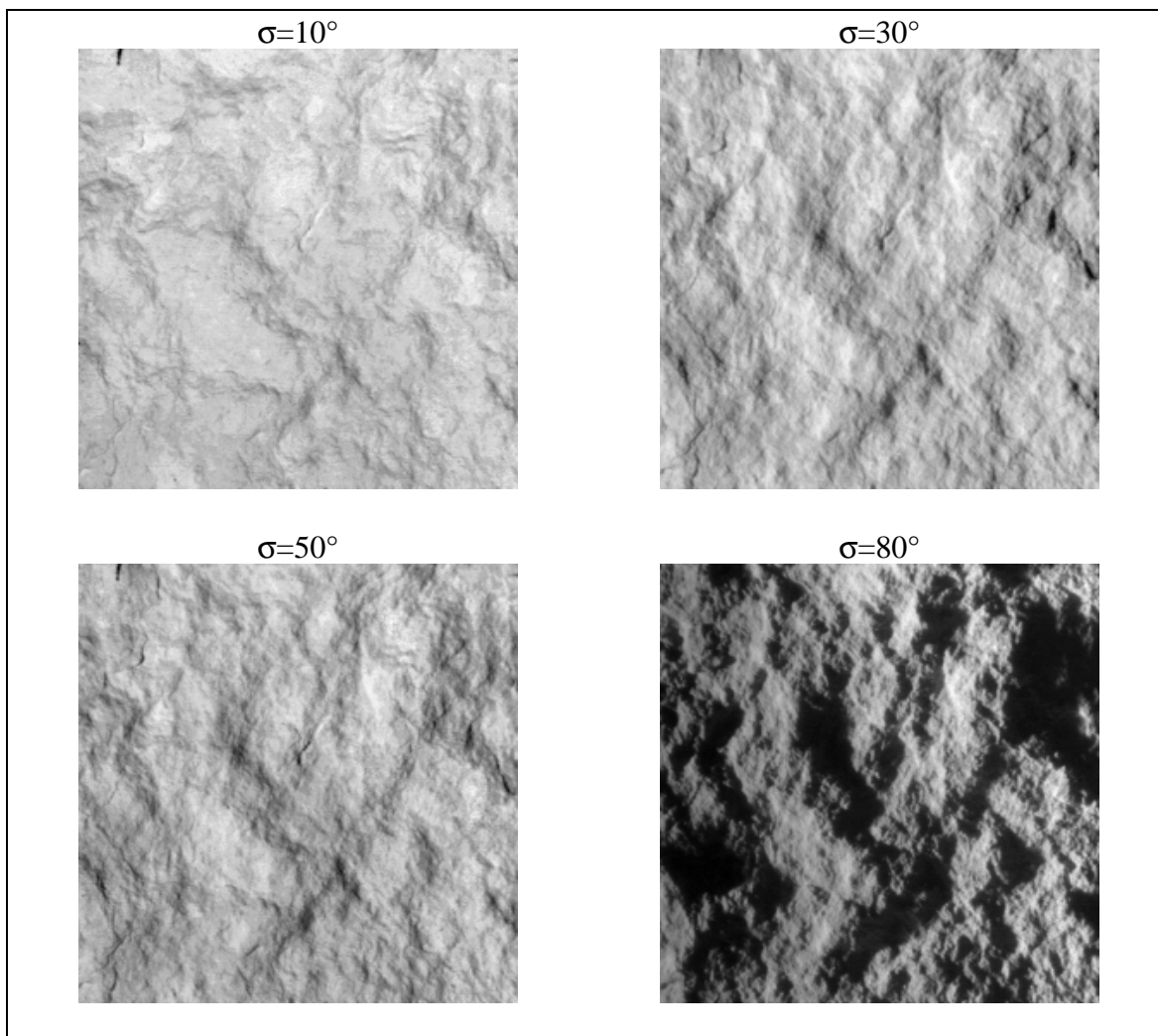
Figure 3.34 - Intensity images of rock1 showing variation with slant angle
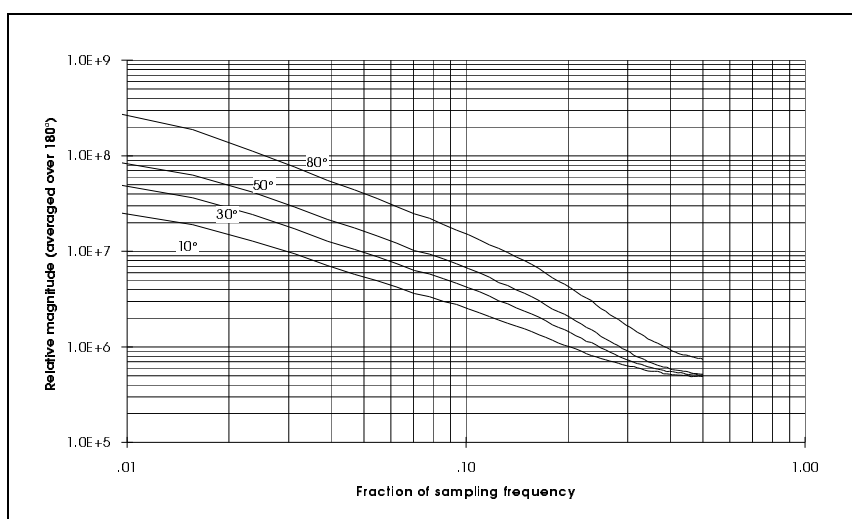
Figure 3.35 - rock1 : slant angle response (σ = 10ᶜ, 30ᶜ, 50° & 80ᶜ)

Figure 3.35 of average radial sections of *rock1's* magnitude spectrum shows that image

variance does increase with slant angle. It is however difficult to assess whether or not it

follows the sin σ relationship (2.17) derived in chapter 2. Estimation of the magnitude at a particular frequency via a straight line approximation is not appropriate here, as radial sections of spectra of the test textures are not straight lines. Hence a simple alternative was employed : the average of the coefficients in the range $\omega = 0.05\omega_S$ to $0.2\omega_S$ was taken. These magnitude estimates were plotted as before against sin σ, and are shown below in figure 3.36.
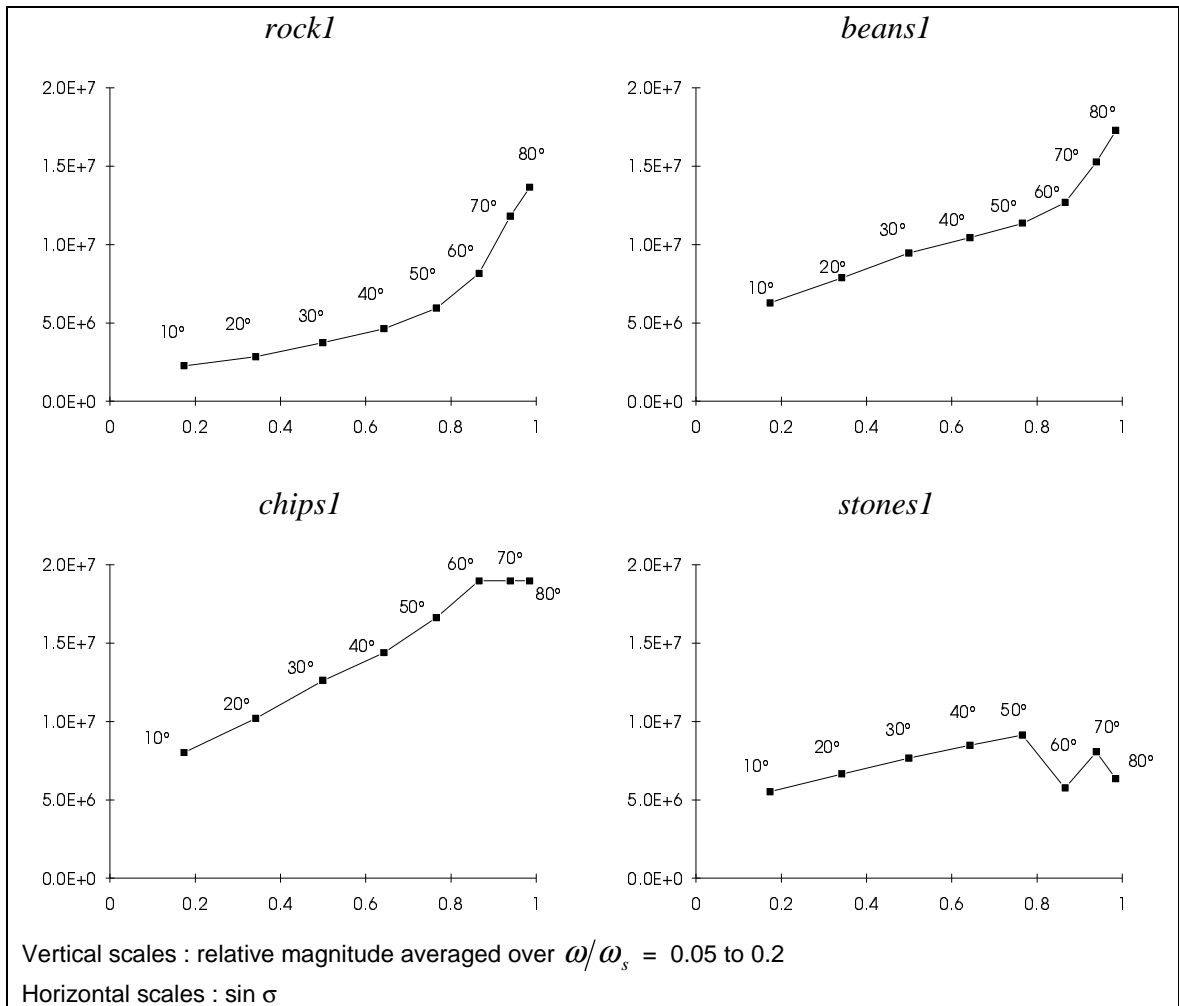
Figure 3.36 - Magnitude estimates vs. sin (σ)

Clearly the graphs above do not display a linear relationship over the entire range of slant angle. However, for the lower values of slant ($\sigma \leq 50°$), where the shadowing has less effect, the graphs do show a sin σ relationship.

3.3.4. Radial shape - slant angle response

The above has shown that, with respect to the test textures, the values of magnitude spectra are *dependent* upon slant angle, and that a sine relationship holds for slant angles of 50° or less. The image model developed in chapter 2 predicted that radial shape is an *intrinsic* property of texture, and therefore *independent* of illuminant slant σ. Figure 3.37 allows the intrinsic nature of this characteristic to be assessed for the four test textures. It shows radial sections through the two dimensional magnitude spectra, at θ = 0° for four values of illuminant slant. It can be seen that the shapes of the graphs do not change significantly with variation in illuminant slant. However, as with the tilt angle response, the plots again converge towards the Nyquist frequency, and except for *stones1,* their gradients are not independent of σ. Hence estimates of the power roll-off factor β_1, are unlikely to provide a texture measure which is purely a function of the surface relief.

σ = 10°(bottom trace), 20° (2nd bottom), 40° (2nd top) & 60°(top trace),
θ = 0°, vertical scales : relative magnitude, horizontal scales : fraction of sampling frequency.
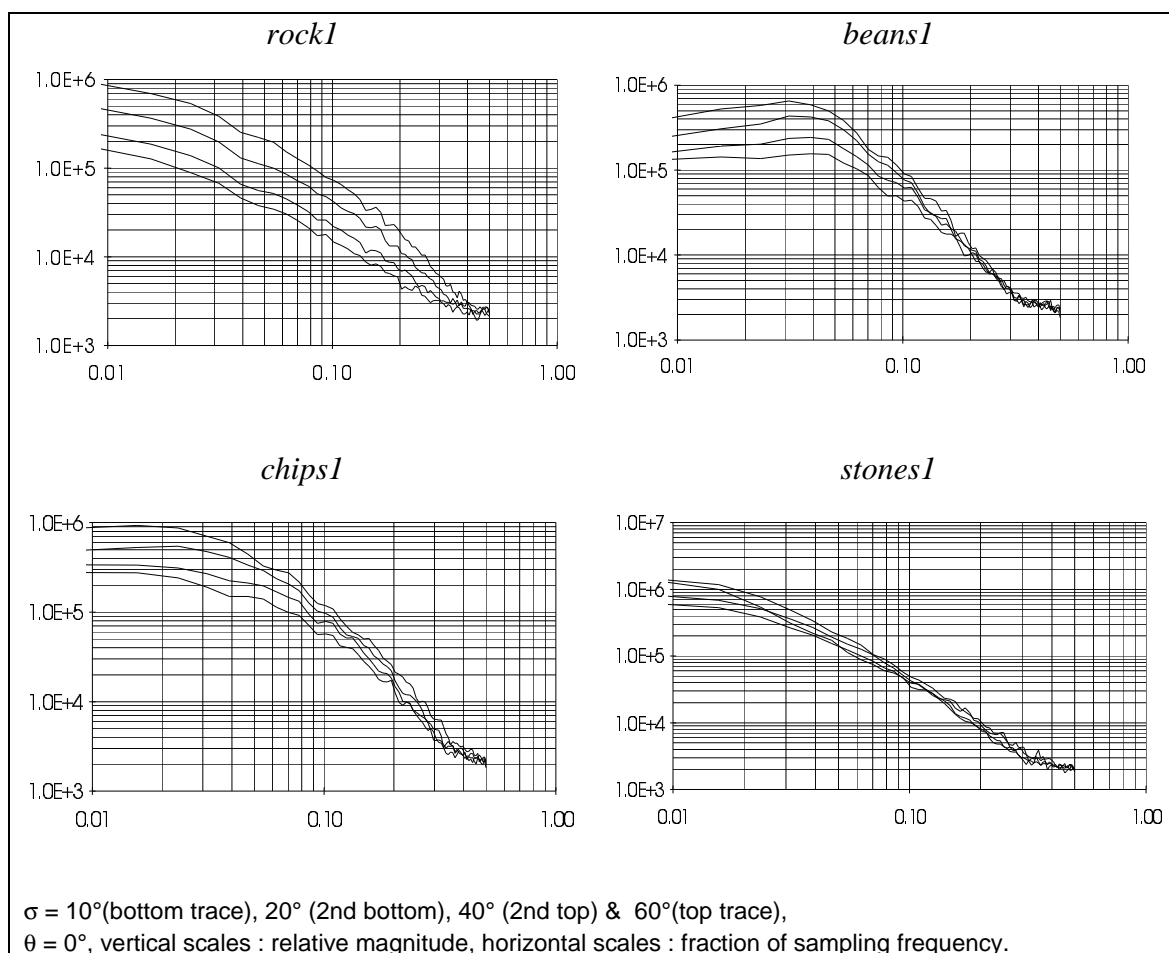
Figure 3.37 - Radial shape : slant angle (σ) response.

3.3.5. Summary of slant response investigation

This section has investigated the slant angle (σ) response of image texture.

- The results of simulation and laboratory experiment have shown that image magnitude spectra are not independent of the illuminant's slant angle.

- In simulation, shadowing severely affected the predicted "sin σ" relationship.

- Laboratory experiments have shown that the slant angle responses of the four test textures, approximates a linear function of sin σ for slant angles of up to 50°.

- Laboratory experiments have also shown that the gross radial shape of magnitude spectra of the four test textures, is unaffected by illuminant slant. However, the gradients of these spectra (and hence the power roll-off factors) are not independent of illuminant slant.

3.4. Conclusions

This section summarises the investigations reported in this chapter and briefly assesses their likely impact on texture classification and segmentation.

Chapter 2 presented an image model of topological texture due to Kube and Pentland [Kube88]. This model is important to texture classification and segmentation as it predicts that many texture features will be affected by changes in illuminant direction. However, the model was derived assuming that slope angles are low, and shadowing was ignored. Thus the purpose of this chapter was to investigate the model's validity particularly with regard to these two aspects.

Chapter 2 divided the model into three parts corresponding to

(i)   the response of image texture to changes in surface relief,

(ii)   the response of image texture to changes in the tilt angle of the illuminant (τ), and

(iii) the response of image texture to changes in the slant angle of the illuminant (σ).

Hence this chapter reported results from three investigations; one for each type of response. The main conclusions from each of these are repeated below :

a) **The response of image texture to changes in surface relief**

The investigation into the effect of surface relief on image texture used an isotropic fractal model of topological texture. For such surfaces the radial shape of the surfaces' PSD plot is of the form $f^{-\beta_H}$ and the image model (2.14) predicts that the radial shape of the image's PSD plot will be of the form $f^{-\beta_I}$, where $\beta_I = \beta_H - 2$ (the β relationship). Results showed that in simulation :

- the β relationship is representative over a range of surface variances, and

- the β relationship is still valid when shadowing occurs.

These results therefore, also support the surface response component of the image model (2.14), from which the β relationship was derived.

b) **The response of image texture to changes in the tilt angle of the illuminant**

The second component of the image model (2.14) predicts that the tilt response of a texture is of the form :

$$F_\tau = \cos(\theta - \tau)$$

Simulation and laboratory experiment were used to investigate this response :

- Results from simulation and experiment show that the directional characteristics of image texture are not intrinsic, but are dependent upon illuminant tilt.

- The results of simulation and laboratory experiment, show that a *raised* cosine (3.8) : $F_\tau = m_\tau \cos(\theta - \tau) + b_\tau$, rather than the straight cosine relationship above, provides a more accurate representation of the tilt response.

c) **The response of image texture to changes in the slant angle of the illuminant**

The third component of the image model (2.14) predicts that the slant response of a texture is of the form :

$$F_\sigma = \sin \sigma$$

As for the previous response both simulation and laboratory experiment were used in the investigation. They showed that :

- the variance of image texture is not an intrinsic characteristic as it is dependent on the slant angle of the illuminant,

- that shadowing severely affects the predicted $\sin \sigma$ relationship, and

- that for the four test textures the slant angle response follows a sine law for values of slant angle less than or equal to 50°.

d)   The intrinsic nature of PSD radial shape

Chapter two's linear image model (2.14) implies that the radial shape of power and magnitude spectra are independent of the illuminant's direction. This characteristic was investigated during slant and tilt experiments. Both showed that the gross shapes of radial sections of the test textures are invariant to the direction of the illumination. However their gradient is affected by variation in the illuminant vector. Hence estimates of the power roll-off factor would not provide a texture feature which is invariant to changes in the orientation of the illuminant.

3.4.1. Implications for texture classification

Many of the feature sets surveyed in chapter 4 contain directional texture measures. In addition some are clearly a function of image variance (see chapter 4). Hence two of the most important of the above conclusions are that

(i)   the directionality of image texture is not solely a function of surface directionality, but that it is also a function of illuminant tilt, and

(ii)   that variation in illuminant slant, can also affect image variance.

Thus classification accuracy may well be reduced if the direction of the illumination either (a) changes between training and classification sessions, or (b) varies over a scene due, for instance, to the proximity of the lighting source.

The purpose of the next chapter therefore, is to review and choose sets of texture features for investigation as to the effects of variation of illuminant direction.